Transworld Research Network
37/661 (2), Fort P.O., Trivandrum-695 023, Kerala, India

Recent Res. Devel. Applied Phys., 5(2002): 27-68 ISBN: 81-7895-047-2

Recent advances in continuous-wave laser difference-frequency generation in the mid-infrared: *State of the art, applications, and perspectives*

Weidong Chen[1], Daniel Boucher[1] and Frank K. Tittel[2]
[1]Laboratoire de Physicochimie de l'Atmosphere, UMR du CNRS 8101, MREID-Universit'e du Littoral Cote d'Opale, 145, Av. Maurice Schumann, 59140 Dunkerque, France, [2]Rice University MS 366, Electrical & Computer Engineering Department, P.O. Box 1892, Houston Texas 77251-1892, USA

Abstract

Recent developments in nonlinear optical materials and laser technology have led to the development of continuous-wave (cw) coherent infrared radiation sources based on nonlinear difference-frequency generation (DFG). Broadly tunable cw laser-based infrared radiation can be generated from 3 to 20 μ m by difference-frequency mixing of visible or near infrared lasers in nonlinear optical crystals. The principle of nonlinear optical generation of infrared coherent light, the state of the art of related techniques encountered in phase-matching schemes, power conversion efficiency, phase-matched DFG, and future potential extension of phase- matchable infrared spectral coverage are discussed. Applications of this type of tunable mid-infrared coherent light source to high-

Correspondence/Reprint request: Dr. Weidong Chen, Laboratoire de Physicochimie de l' Atmosphère, UMR du CNRS 8101 MREID- Université du Littoral Côte d'Opale, 145, Av. Maurice Schumann, 59140 Dunkerque, France
Tel: 33 3 2865 8264, Fax: 33 3 2865 8244

resolution spectroscopic analysis of chemical trace gas species are presented.

1. Introduction

Nonlinear optical frequency down-conversion by means of a $\chi^{(2)}$ parametric interaction process, such as difference-frequency generation (DFG) and optical parametric oscillation (OPO), can be employed to generate coherent light at mid-infrared wavelengths for which there exist no convenient direct laser sources.

In this paper we emphasize continuous-wave (cw) DFG techniques (for a recent review of optical parametric oscillators the reader is referred to a review article by Dunn et al [Dunn99]). Continuous-wave nonlinear frequency conversion source based on difference-frequency generation in the infrared was first reported by Pine [Pine 74] in 1974 for use in high-resolution spectroscopy. Infrared radiation at 3 μm with a power level of ~ 0.5 μW was generated by DFG of a single mode Ar^+ ion laser mixed with a single mode cw dye laser in a 5-cm long $LiNbO_3$ crystal. Oka [Bawe90] replaced $LiNbO_3$ by a $LiIO_3$ crystal thereby achieving a spectral coverage from 3 to 5.2 μm. Extension of the infrared spectral coverage to mid- and long- infrared wavelengths using DFG was initially limited by the availability of effective pump lasers and suitable nonlinear optical materials in the 1970 and 1980s.

Since 1990, there has been a renaissance in mid-infrared DFG performance as a result of significant advances in nonlinear optical materials, pump laser and photonics technology. The availability of new nonlinear optical materials, with high optical-quality and large nonlinearity, novel phase-matching schemes, and progress in laser technology (such as single-frequency, room temperature diode lasers, diode pumped solid-state lasers, fiber amplifiers and lasers, and broadly tunable Ti: Sapphire lasers) have led to new opportunities in the developments of cw tunable coherent radiation sources in the 3-20 μm spectral region.

Demonstration of DFG-based infrared sources from 4 to 10 μm at Rice University (Houston) since 1991 [Cana92, Hie192, simo93a, Simo95] represent an important milestone in the recent development of DFG based radiation sources. Wide wavelength tuning has been achieved by mixing two tunable lasers (cw dye, Ti: Sapphire laser) in $AgGaS_2$ crystals. Since1996, $AgGaS_2$ DFG based spectroscopic sources have been reported by several other groups: Chen et al [Chen96], Kronfeldt et al [Kron96], and Schade et al [Scha96]. The development of the laser-based infrared DFG sources have been motivated not only for high- resolution spectroscopy, but for applications in applied spectroscopy such as environmental monitoring of greenhouse gases, toxic chemical species, as well as for medical diagnostics, because most molecular species exhibit strong rational-vibrational absorption features with characteristic chemical bonds (such as C-H, C=O, C-C1, N-H) in the infrared region. A survey of characteristic bond vibrations in the infrared is depicted in Fig.1.

High-spectral purity, wide wavelength tunability and excellent beam quality made this type of spectroscopic source a very attractive alternative to FT-IR spectrometers, infrared lead salt diode and gas lasers. Various cw infrared difference-frequency generation techniques have been recently reported: DFG in birefringent nonlinear crystals including $KTiOPO_4$ [Momo96], $LiNbO_3$ [Seit98], $AgGaS_2$ [Chen98a, Chen98b, Petr98a, Lee98], $AgGaSe_2$ [Petr96a, Sump98] in the 4-18μm spectral region, and GaSe for longer

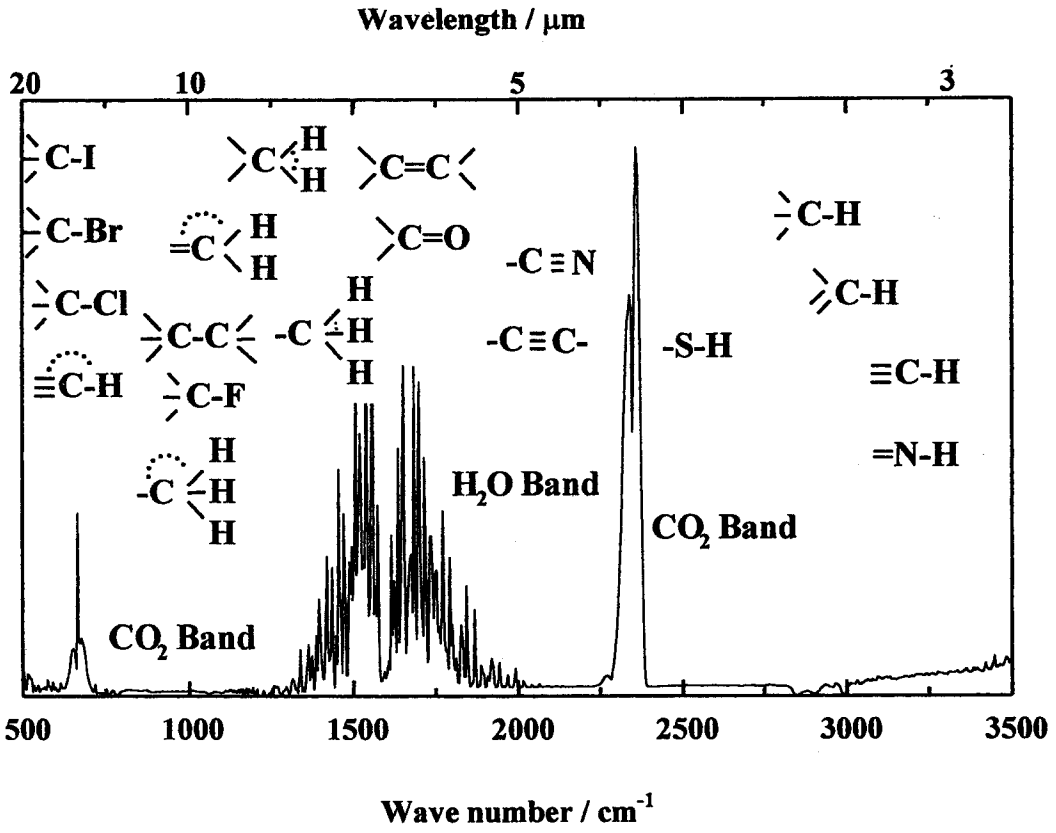

Figure 1. Survey of characteristic infrared bond vibrations of spectroscopic interest

infrared wavelengths from 8 to 19 μm [Eckh96, Chen98c, Putn98]; as well as DFG in periodically poled bulk ferroelectric materials, such as $LiNbO_3$ (PPLN, See, e.g. [Gold95, Petr96b]), $RbTiOAsO_4$ (PPRTA, [Frad00a, Chen01a]), $KTiOPO_4$ (PPKTP, [Frad99]), $KTiOAsO_4$ (PPKTA, [Frad00b]) for 3-5 μm wavelength region, DFG in waveguide $LiNbO_3$ based devices [Chou98, Petr98b] and GaAs for the 2-14 μm spectral region [Fior97, Zhen98, Eyre99].

2. Background

In this section we shall summarize the principle of mid-infrared generation by difference-frequency down-conversion, since the theoretical considerations have been treated by numerous authors (e.g. [Butc90, Boyd92]).

2.1. Mid-infrared radiation by difference-frequency generation

When intense electromagnetic waves propagate through a nonlinear optical material, the polarization **P** induced by the applied electric field **E** can be expressed as:

$$\mathbf{P}(t) = \chi^{(1)}\mathbf{E}(t) + \chi^{(2)}\mathbf{E}^2(t) + \chi^{(3)}\mathbf{E}^3(t) + \ldots\ldots \quad (1)$$

where the quantities $\chi^{(1)}$, $\chi^{(2)}$, and $\chi^{(3)}$ are referred the linear, the second – and third-order nonlinear optical susceptibilities, respectively. In the case of three waves parametric

mixing, the driving field consists of two distinct frequency components ω_1 and ω_2:

$$\mathbf{E}(t) = \mathbf{E}_1 e^{-j\omega 1t} + \mathbf{E}_2 e^{-j\omega 2t} + \mathbf{c.c.} \quad (2)$$

The time-varying polarizations act as the source for the generation of a new electromagnetic field, as described by the following wave equation based on Maxwell wave equation:

$$\nabla^2 E - \varepsilon_0 \mu_0 \frac{\partial^2 E}{\partial^2 t} = \mu_0 \frac{\partial^2 P}{\partial t^2} \quad (3)$$

Difference-frequency generation is a frequency down-conversion process by the nonlinear polarization $\mathbf{P}(\omega_1 - \omega_2) = 2\chi^{(2)} \mathbf{E}_1 \mathbf{E}_2^*$ which gives rise to a new electromagnetic field at the difference-frequency of the two incident waves $\mathbf{E}_1$ and $\mathbf{E}_2$ via $\chi^{(2)}$ nonlinear parametric interaction in a nonlinear optical crystal. This process can be schematically shown in Fig. 2. A "signal" photon (at frequency ω_s) stimulates the break down of a "pump" photon (at frequency ω_p) into "signal" and "idler" photons (at an infrared frequency $\omega_i = \omega_p - \omega_s$) satisfying the laws of conservation of photon energy and momentum. The subscripts s, p, i refer to the signal, pump, and idler (infrared), respectively.

Due to optical frequency dispersion in the refractive index of nonlinear crystals, the interacting waves at different frequencies travel at different velocities (defined as c/n (ω), where c is the speed of light and n(ω) is the frequency-dependent refractive index). The difference in the phase velocities produces a phase difference that accumulates along the length of the nonlinear device. The relative phases of the interacting waves determine the

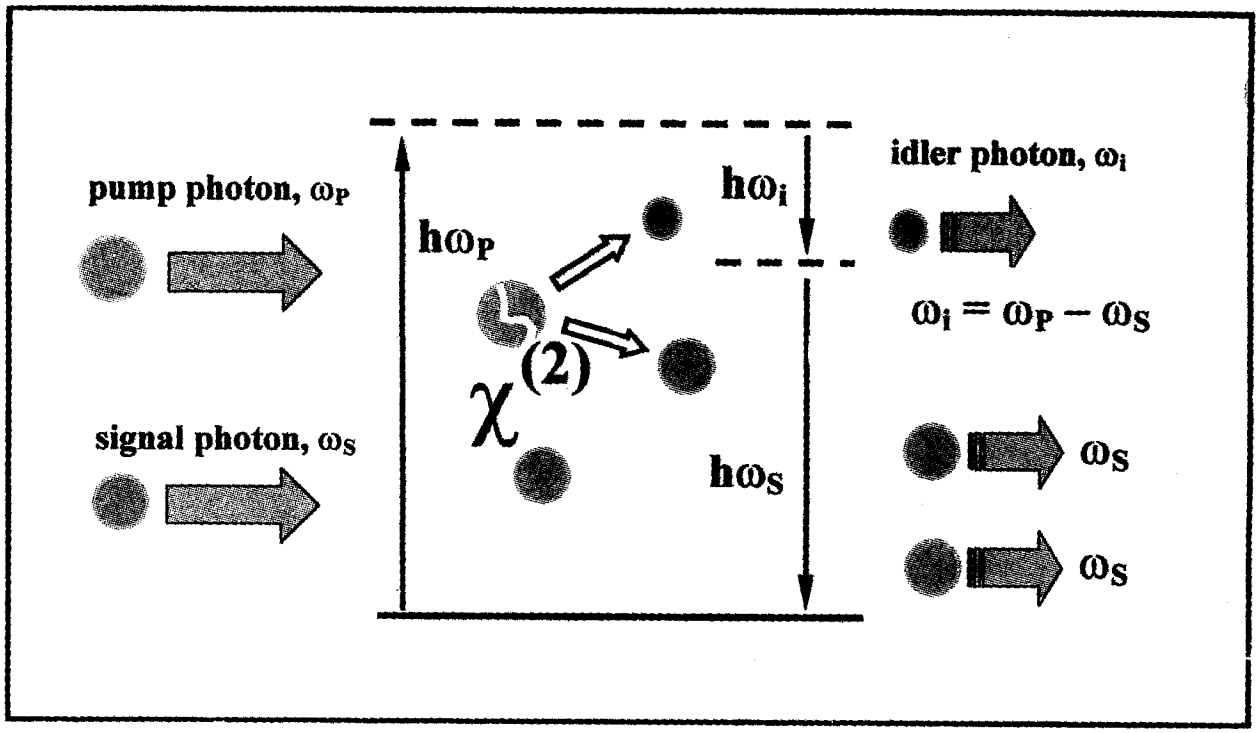

Figure 2. DFG by a $\chi^{(2)}$ nonlinear optical parametric interaction process

direction of the generated power flow. A phase shift of π is produced over every coherence length, which can lead to a reversal of the energy flow between the driving and generated waves. For efficient frequency conversion, the critical requirement is that the interacting waves must stay in phase along their path through the nonlinear medium. This requirement is usually referred to as phase-matching (PM) [Arms62]. The nonlinear generation power at the resultant frequency ω_i is given by

$$P_i = \eta \cdot P_p \cdot P_s \cdot L^2 \ \mathrm{sinc}^2 (|\Delta \mathbf{k}| L / 2) \quad (4)$$

assuming a plane wave approximation, and where $\mathbf{k}$ is the wave sector within the nonlinear optical medium and $\Delta\mathbf{k}$ describes the phase mismatch resulting from unequal phase velocities of the interacting waves; η is the power conversion coefficient, L is the waves interaction length inside the nonlinear material, P_p and P_s are the pump and signal laser powers, respectively. The wave vector mismatch $\Delta\mathbf{k}$ is given by:

$$\Delta \mathbf{k} = \mathbf{k}_p - \mathbf{k}_s - \mathbf{k}_i \quad (5)$$

The maximum frequency conversion efficiency can be obtained when the phases of the interacting waves are matched so that $\Delta\mathbf{k}$=0. Fig.3 depicts the phase-mismatching effect of the DFG process in an $AgGaS_2$ crystal [Chen96]. The experimental curve (a) is compared with a sinc^2 function (b), which describes the effects of phase-mismatch, based on a plane-wave model. The asymmetry of the experimental curve is due to interaction effect of focused Gaussian beams [Chu85, Zond98].

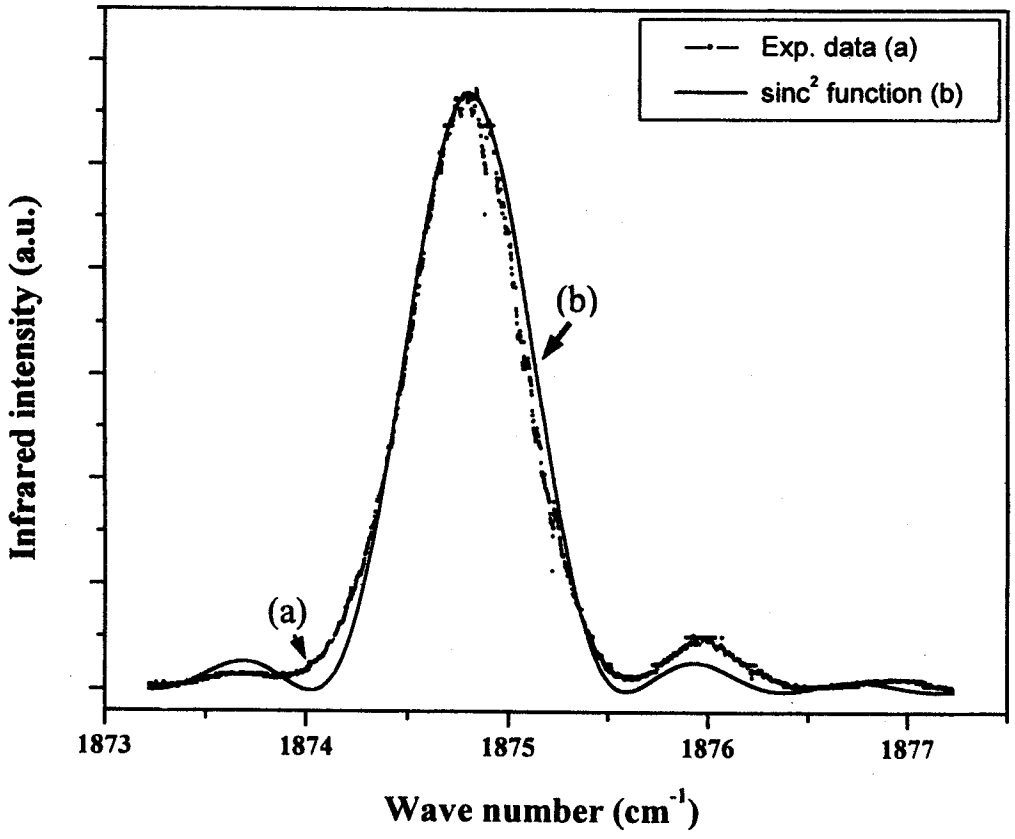

Figure 3. Infrared frequency DFG detuning characteristics of $AgGaS_2$: (a) experimental; (b) sinc^2 function that considers phase mismatch in the frequency conversion process.

2.2. Phase-matchable nonlinear optical materials for the mid-infrared

The success of any nonlinear optical process depends upon compensating for the wavelength-dependent dispersion of the phase velocities, i.e. offsetting the effect of dispersion so that the three interacting waves travel in synchronism inside the crystal medium. This can be achieved by different phase-matchable nonlinear optical materials, as listed below:

1) Birefringent Phase-matachable (BPM) crystals. These include such materials as $LiNbO_3$, $AgGaS_2$, $AgGaSe_2$, GaSe, and $ZnGeP_2$. In this kind of material, birefringence is used to adjust the different phase velocities by matching the field polarizations of the different mixing waves to the phase-matching required crystal axis (if the signal and idler have the same polarization, this phase matching is referred to *type I* PM; while the case of different polarizations for the signal and idler corresponds to a *type II* interaction). For this purpose orthogonal polarizations between interacting waves are required with an appropriate combination of the pump and signal wavelengths. Figure 4 shows BPM curves of several commercially available nonlinear crystals useful for DFG in the mid-infrared spectral region.

Phase-matching using birefringence requires finding a concidence between the birefringence-dependent wavelengths of interest and those available from pump sources which satisfies $\Delta k=0$ and fall within the optical transmission range for a given crystal. This requirement restricts the number of crystals suitable for nonlinear frequency conversion to only about ten commercially available crystals for infrared DFG applications [Eksm].

2) Quasi-phase-matchable (QPM) bulk crystals. A quasi-phase matching technique was first proposed by Armstrong et al in 1962 [Arms62]. In a QPM scheme, periodic structures are used to offset the accumulated phase mismatch: the signs of the optical nonlinearity of the crystals are modulated along the propagation direction so that the phase is periodically reset by π with a half-period equal to the coherence length. Two techniques have been implemented: (1) a photolithographically patterning method [Burn94, Myer99], which is used for electric-field poling of ferroelectric materials (such as $LiNbO_3$, $KTiOPO_4$, $RbTiOAsO_4$, $LiTaO_3$, $KTiOAsO_4$) to provide precise periodical domain sizes ranging from 5 to 30 μm; (2) Epitaxial orientation patterned growth [Eyre99] or diffusion stacking-bonding [Miss98] methods, which are applied to III-V semiconductors (such as GaAs, ZnSe).

Fig.5 shows a microphotograph of an etched grating domain pattern of a PPRTA crystals [Chen01a].

In contrast to BPM, as the QPM materials can be engineered to be phase-matchable at any wavelengths within the transparency range of the crystal by selecting the appropriate modulation period Λ. This method allows a free choice of polarization of the interacting waves and the use of the largest nonlinear susceptibility component. Moreover, as the QPM scheme does not rely on birefringence, it can be used in isotropic materials with a large optical nonlinearity. The DFG power conversion efficiency in QPM bulk ferroelectric crystals, such as periodically poled $LiNbO_3$ (PPLN) is typically of the order 0.01% $W^{-1}cm^{-1}$, which is usually one order of magnitude higher than that obtained in the BPM-DFG process.

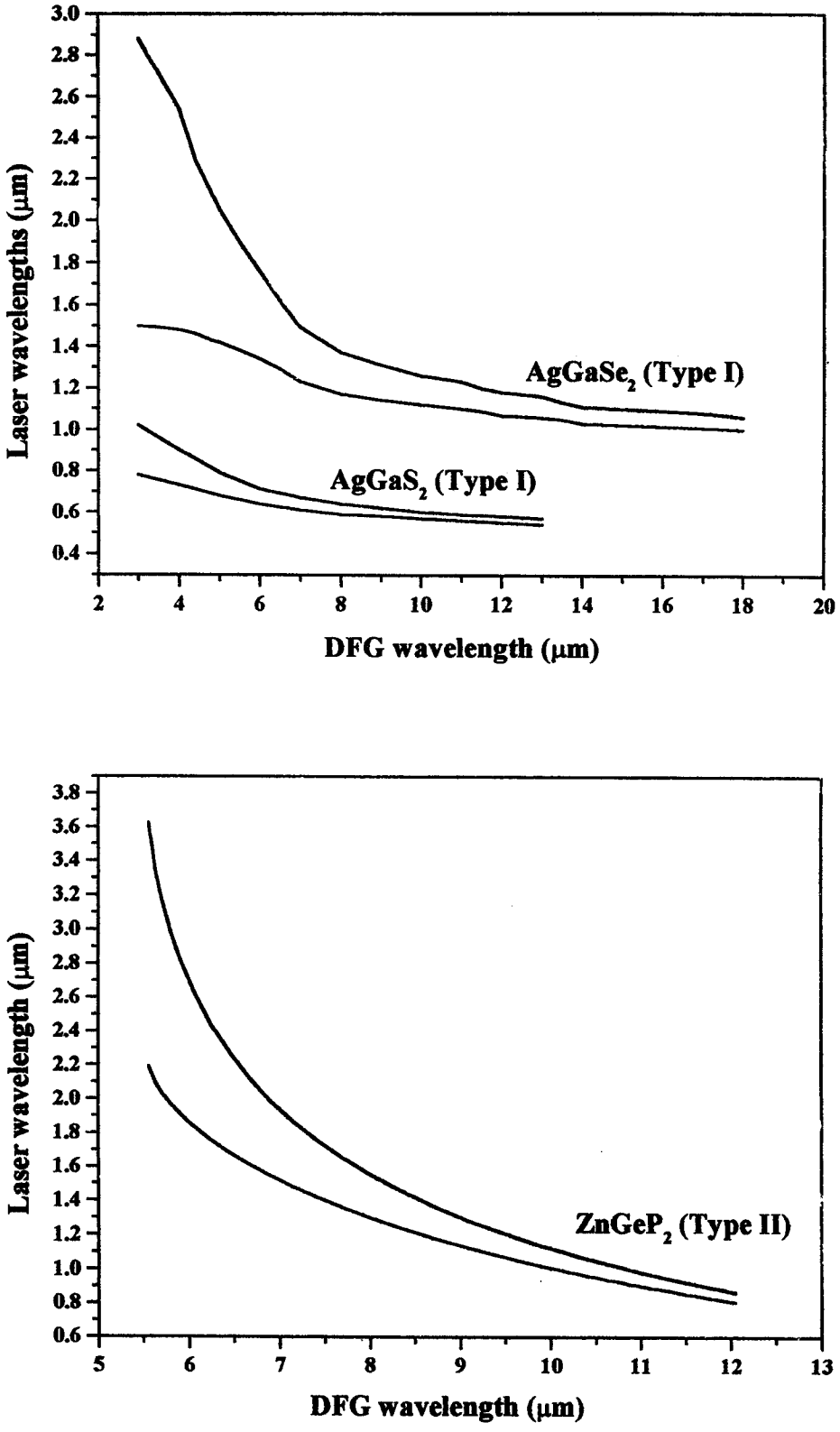

Figure 4. Birefringent phase-matchning characteristics of $AgGaS_2$, $AgGaSe_2$, and $ZnSeP_2$ crystals. DFG driven by visible and/or near-IR pump lasers can produce a wide range of tunable mid-infrared radiation from 5 to 20 μm.

Figure 6 shows a QPM curve of infrared generation from 3 to 5.5μm in a PPLN

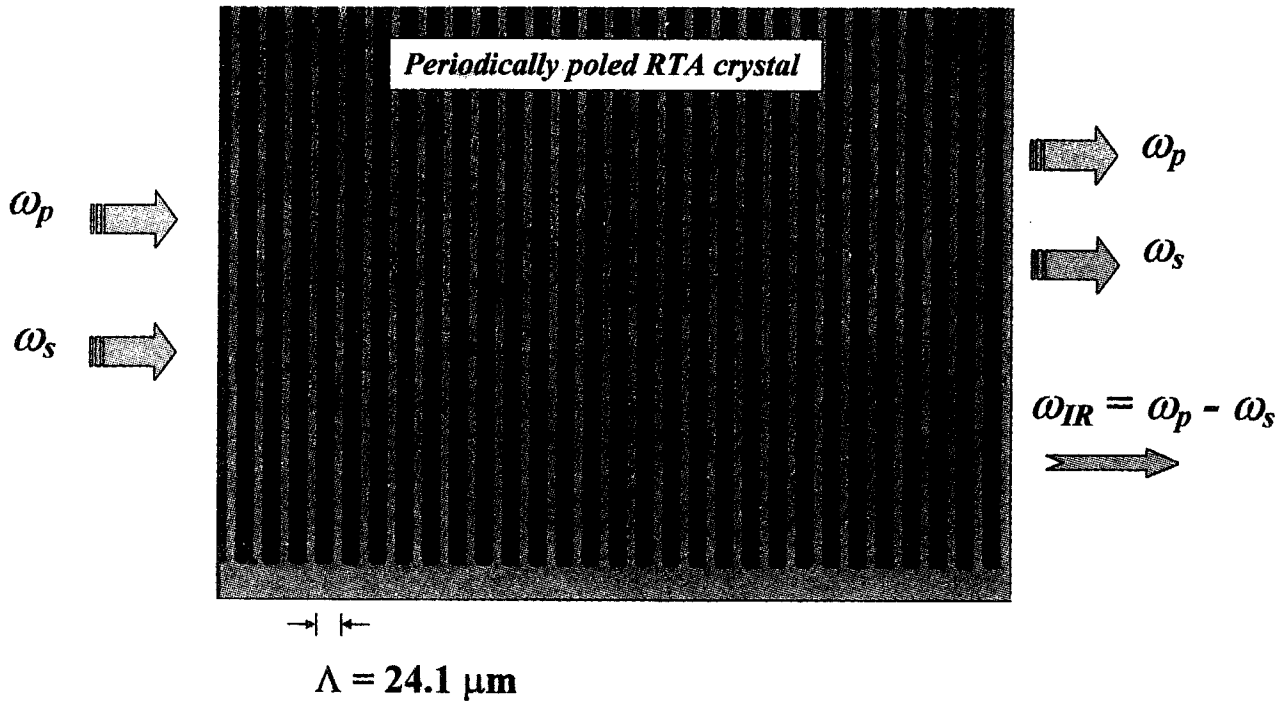

Figure 5. A side view microphotograph (100X) of an etched PPRTA grating pattern, taken with a polarization optical microscope (Leitz DM RXP).

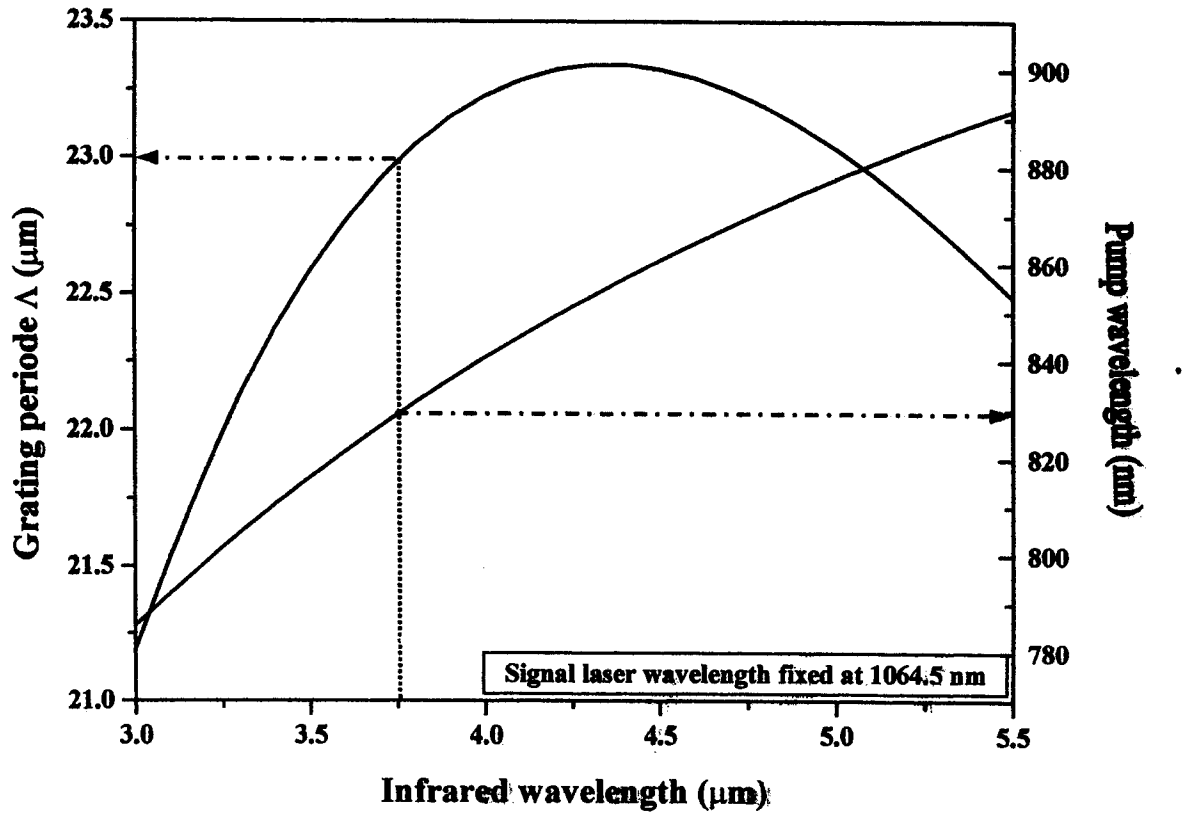

Figure 6. Characteristics of QPM-DFG in a PPLN crystal at room temperature. Shown is the generated infrared wavelength as a function of the pump laser wavelength and the grating period Λ (with the signal laser fixed at 1064.5 nm). The pump wavelengths combination and the QPM grating period for the infrared DFG at ~ 3.75 μm are ~ 830 nm, 1064.5 nm and 23μm, respectively.

crystal pumped by a signal laser fixed at 1064.5 nm and pump laser tunable from 785 to 892 nm.

3)Waveguided QPM materials. The efficiency of traveling-wave bulk interactions is restricted by a trade-off between tight focusing for high laser intensities and loose focusing for large interaction lengths. Dielectric waveguided nonlinear materials, such as waveguided PPLN [Lim91, Bort94, Chou98] and GaAs [Fior97, Zhen98], offer guided interacting waves inside the nonlinear media, which minimize diffraction effects. Hence, single-pass frequency conversion efficiencies are two or three orders of magnitude (up to 100% W^{-1} for some devices [Arbo96, Chou98, Hofm99]) larger than that obtained with single-pass interaction in a bulk crystal. Waveguided QPM based device can be fabricated by using one of the following techniques: (1) periodic structured QPM [Yoo96, Petr00]; (2) waveguide modal dispersion or index birefringent PM [Brav98] and (3) Cerenkov PM [Avet99].

In summary, an effective nonlinear optical material suitable for frequency-down conversion should be optically transparent at the three frequencies of the interacting waves, phase matchable with a larger nonlinear coefficient $\chi^{(2)}$ and a high optical damage threshold. Also important are optical homogeneity, mechanical and thermal properties, and commercial availability.

Table I lists the principal nonlinear optical media currently used for DFG applications in the 3 to 20 μm region, that are phase-matchable by both birefringence, and quasi-phase-matching.

A good review of nonlinear materials for optical frequency conversion can be found in reference [Bord93, Rama93, Myer99].

2.3. Phase-matching techniques and Sellmeier equation

2.3.1. Phase-matching techniques

(1) Wavelength tuning: The wavelengths of the pump and signal lasers are selected so that the wavelength-dependent refractive indices at each of the three interacting frequencies are phase-matched. It is evident that at least one of the two pumping lasers should be tunable in wavelength and their polarizations should be phase-matched as required by the crystal orientation (See Fig.4).

(2) Temperature tuning: Phase-matching can also obtained by adjusting the temperature-dependent refractive indices. This technique is useful when the birefringence of the crystal is strongly sensitive to temperature and if fast tuning is not required.

(3) Angle tuning: The refractive indices can be varied by the angular orientation of the crystal optic axis with respect to the propagation direction of the incident pump laser beams. This method, however, may introduce "walk-off" effects of the Poynting vector for the extraordinary wave due to double refraction. This effect leads to a reduction of the spatial overlap between the interacting waves, and thus degrades the parametric conversion efficiency.

(4) Quasi-phase-matching: The sign of the nonlinear susceptibility is periodically altered along the length of the medium to ensure that the pump energy monotonically

Table I. Properties of some important phase-matchable nonlinear materials [Dmit97], and (a): [Suth96], (b): [Shoj97]

Crystal	Nature	Transparency (μm)	Nonlinear coefficient (pm/V)	Damage threshold (MW/cm^2)
$LiIO_3$	$n_o > n_e$	0.28 - 6	d_{33}=4.5 (@ 1.064 μm)	120 (@ 1.064 μm & 10 ns)
$K_3Li_2Nb_5O_{15}$	$n_o > n_e$	0.35 - 5	d_{31}=5.8 (@ 1.064 μm)	-
Ag_3SbS_3	$n_o > n_e$	0.7 - 14	d_{22}=8.2 (@ 10.6 μm)	46 (@10.6 μm & 200 ns)
Ag_3AsS_3	$n_o > n_e$	0.6 - 13	d_{31}=10.4 (@ 10.6 μm)	46 (@ 10.6 μm & 190 ns)
$KTiOPO_4$	biaxial	0.35 – 4.5	d_{33}=10.7 (@ 1.064 μm)	150 (@ 1.064 μm & 20 ns)
$AgGaS_2$	$n_o > n_e$	0.47 - 13	d_{36}=11.1 (@ 10.6 μm)	10 (@ 10.6 μm & 150 ns)
$RbTiOAsO_4$	biaxial	0.35 – 5.8	d_{33}=12.1 (@ 1.064 μm)	400 (@ 1.064 μm & 10 ns)
$KTiOAsO_4$	biaxial	0.35 – 5.3	d_{33}=16.2 (@ 1.064 μm)	1200 (@ 1.064 μm & 8 ns)
Banana	biaxial	0.37 - 5	d_{33}=16.5 (@ 1.064 μm)	4 (@ 1.064 μm & 450 ns)
CdSe	$n_e > n_o$	0.75 - 25	d_{31}= -18 (@ 10.6 μm)	60 (@ 10.6 μm & 200 ns)
$CsTiOAsO_4$	biaxial	0.35 – 5.3	d_{33}=18.1 (@ 1.064 μm)	-
$KNbO_3$	biaxial	0.4 - 4	d_{33}= -20.6 (@ 1.064 μm)	150 (@ 1.064 μm & 25 ns)
$HgGa_2S_4$	$n_o > n_e$	0.55 - 13	d_{36}=24 (@ 1.064 μm)	60 (@ 1.064 μm & 30 ns)
$LiNbO_3$	$n_o > n_e$	0.4 – 5.5	d_{33}= -27 (@ 1.06 μm)	100 (@ 1.064 μm & 20 ns)
$AgGaSe_2$	$n_o > n_e$	0.71 - 19	d_{36}=33 (@ 10.6 μm)	10 (@ 10.6 μm & 150 ns)
HgS	$n_e > n_o$	0.62 - 13	d_{11}=50 (@ 10.6 μm)	40 (@ 1.06 μm & 17 ns)
GaSe	$n_o > n_e$	0.62 - 20	d_{22}=54 (@ 10.6 μm)	30 (@ 10.6 μm & 125 ns)
Tl_3AsS_3	$n_o > n_e$	1.28 - 17	d_{+}=67.5 (@ 10.6 μm)	10 (@ 10.6 μm & 150 ns)
$ZnGeP_2$	$n_e > n_o$	0.74 - 12	d_{36}=68.9 (@ 10.6 μm)	3 (@ 1.064 μm & 10 ns)
Se	$n_e > n_o$	0.7 - 21	d_{11}=97 (@ 10.6 μm)	-
$CdGeAs_2$	$n_e > n_o$	2.4 - 18	d_{36}=282 (@ 10.6 μm)	33 (@ 10.6 μm & 150 ns)
Te	$n_e > n_o$	3.5 - 36	d_{11}=598 (@ 10.6 μm)	2 (@ 10.6 μm & 150 ns)
Waveguided -GaAs	-	1-16	d_{14}=368.7 [(a)] d_{36}=119 [(b)]	-

flows from the pump waves into the generated DFG wave, as described in section 2.2.

In general one technique can be used in combination with another to achieve phase matched DFG with a wide spectral region [Suth96]. Figure 7 depicts phase-matching curves for DFG in GaSe from 8 to 18 μm, obtained by both laser wavelength tuning and crystal external angle tuning of the crystal [Chen00c]. Figure 8 depicts temperature-tuned QPM wavelength of DFG in a PPRTA crystal [Chen01a].

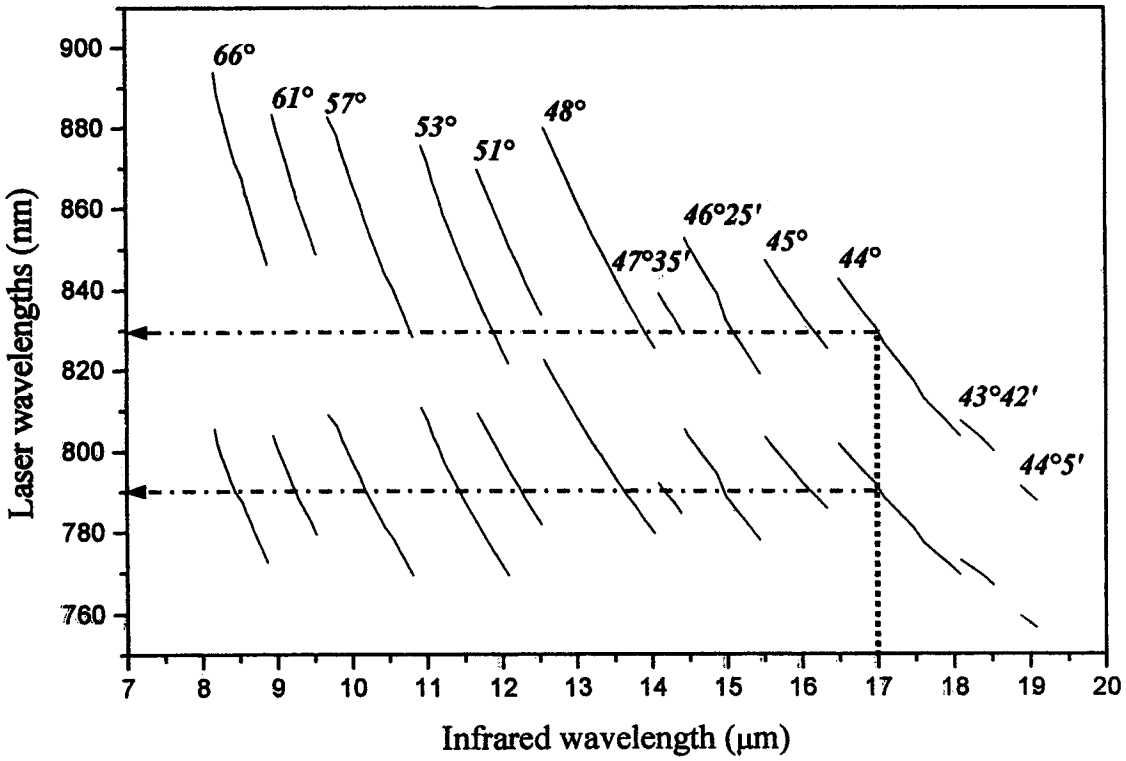

Figure 7. Infrared wavelength tuning characteristics of DFG in a GaSe crystal from 8 to 18 μm, birefringently phase-matched by tuning of laser wavelengths and crystal angle.

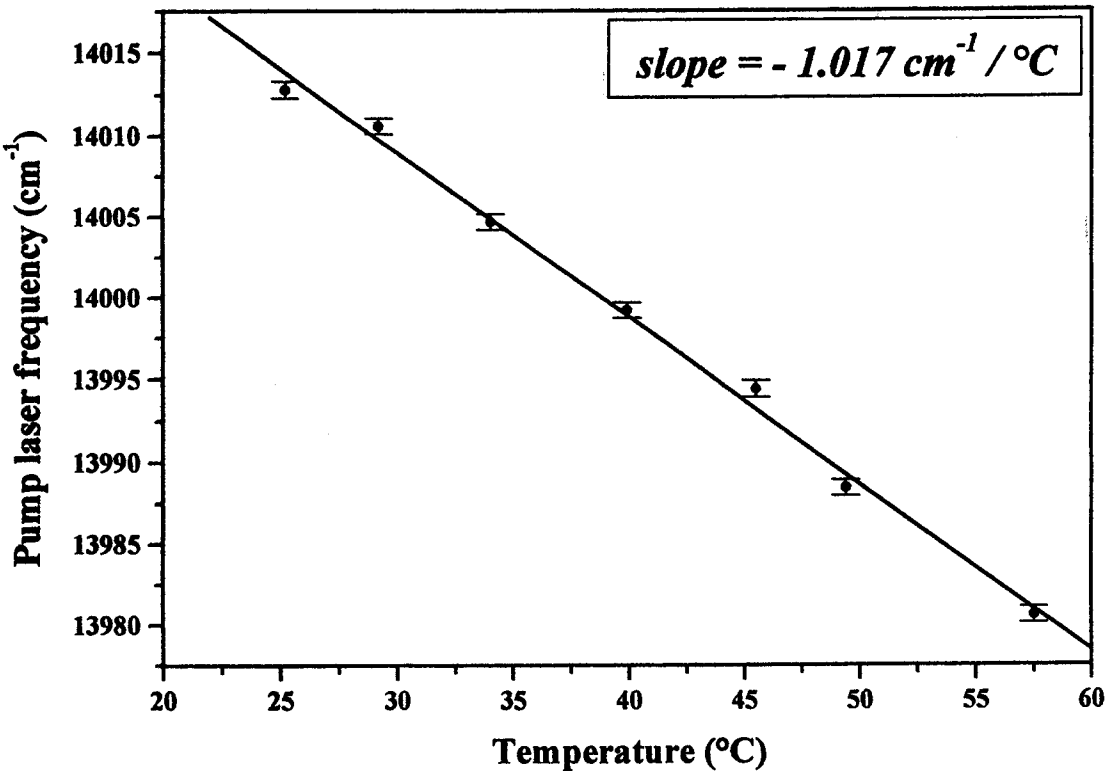

Figure 8. Temperature-dependent QPM wavelength tuning of DFG in a PPRTA crystal. In this experiment, the signal laser was fixed at ~11481 cm^{-1}, and the pump laser was scanned to track the QPM condition.

2.3.2 Phase-matching calculation

Phase - matchable pump laser wavelengths (as well the phase - matchable angle of the nonlinear crystal) are usually calculated using a wavelength-dependent dispersion equation, the so called Sellmeier equation. The dispersion coefficients for most of the commercially available materials can be found in Ref. [Eksm]. For example the Sellmeier equation of PPRTA can be written as [Feni96]:

$$n_z^2(\lambda) = A + \frac{B}{1-(C/\lambda)^2} - D\cdot\lambda^2 \qquad (6)$$

where λ is given in micrometers and A, B, C, D are the Sellmeir coefficients.

The Sellmeier parameters are generally determined by fitting the measured wavelength-dependent indices of refraction with a precision of $\Delta n \sim 10^{-4}$ using a minimum-deviation technique [Bond65, Nels74]. However, this precision is usually not accurate enough. Differences (δv, in cm^{-1}) in the laser frequencies between the predicted values and the experimental data are typically ~100 cm^{-1}. Figure 9 shows experimental QPM laser wavelengths (dots) for infrared generation from 3.4 to 4.5 μm in a PPRTA crystal. The predicted values based on the Sellmeier equation are also plotted for comparison. The offset δv in maximum QPM conversion wavelengths from the theoretically calculated value [Feni96] (dashed lines) was ~ 220 cm^{-1} at 4.5μm. Using cw QPM-DFG data in the

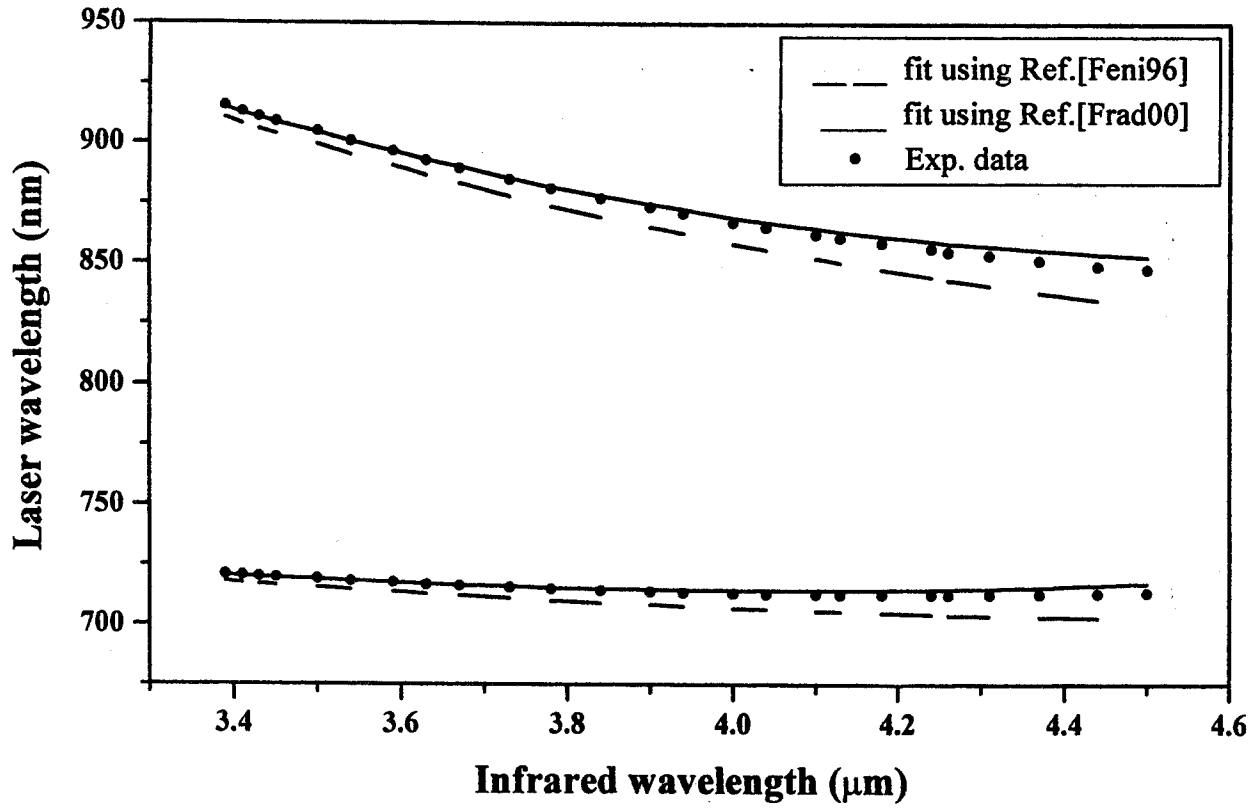

Figure 9. Quasi-phase-matching characteristics of the PPRTA crystal at room temperature. The generated infrared wavelength as a function of the mixed laser wavelengths is shown. The dashed and solid curves represent calculated values based on the Sellmeier equation given in [Feni96] and [Frad00], respectively, and dots indicate experimental data [Chen01a].

1.53-3.48 μm and the measurements given in [Feni96] for the 0.8-1.3μm range, Fradkin-Kashi et al reported an improved dispersion equation [Frad00a], which yielded a maximum offset reduced to be ~73cm^{-1} at 4.5μm (represented by solid lines in Figure 9):

$$n_z^2(\lambda) = A + \frac{B}{1-(C/\lambda)^2} + \frac{D}{1-(E/\lambda)^2} - F\cdot\lambda^2 \qquad (7)$$

In case of DFG in an $AgGaS_2$ crystal, an improved dispersion equation has been obtained by fitting experimental cw PM data. This led to a decrease in the δν value from ~100 cm^{-1} to ~ 5 cm^{-1} in the 4.5-6.2μm spectral region [Chen99].

2.4. Practical laser pump sources suitable for cw DFG bases mid-infrared sources

The spectral features of a DFG coherent light source are characterized by the parameters of the two pump lasers (pump and signal). Hence the following parameters for a laser sources are desirable: (1) narrow pump laser linewidths, preferably single longitudinal mode (since the DFG source linewidth is equal to the convolution of the pump laser linewidths under Gaussian beam profile assumption); (2) wavelength tunability; and (3) sufficient laser pump power in order to generate significant levels of DFG power.

2.4.1 Dye and Ti: Sapphire lasers

Commercially available cw dye and Ti:Sapphire (Ti:Al_2O_3) laser, optically pumped by an Ar+ or frequency converted diode pumped solid state laser (e.g. Autoscan 899-29 system from Coherent Inc.), are widely tunable from the visible to the near infrared (580-1100 nm, [Lfw00]). The high spectral purity (~ 500 kHz, even <100 kHz for the MBR-110 system), significant cw single frequency output power levels (>100 mW and up to several Watts maximum power), wide tunability, and automated continuous wavelength scanning make them suitable pump sources for DFG in $AgGaS_2$, GaSe, PPLN, PPRTA for use in high-resolution infrared spectroscopy in the 3 to 20 μm spectral region.

2.4.2 Diode lasers

Rapidly developments of diode laser performance triggered by the optical telecommunication industry over the last decade exhibit some advantages for DFG based sources: efficient (resulting in low power consumption), compact monolithic device and simple operation. In addition, compared to Fabry-Perot cavity type laser diodes, single-longitudinal mode operation of the diode laser has been dramatically improved by the use of distributed feedback (DFB) and distributed Bragg reflector (DBR) structures, incorporated during the diode laser fabrication process. The wavelength-selective optical feedback forces single frequency laser operation at wavelengths defined by the DFB grating. Numerous types of diode lasers are attractive for application in DFG-based gas sensor instrumentation [Rich00]. The tunability of the DFB- or DBR- based diode lasers, however, are typically limited to a few nanometers. Improvement of the wavelength tuning and linewidth narrowing can be accomplished by using external-cavity structures

[Lang98], where the semiconductor diode is used as a gain element in an external cavity containing a diffraction grating and tuning mirror, which permits wide wavelength tuning within the gain curve of the laser, some tens of nanometers with a narrower linewidth (linewidths ~ 50 kHz as compared to ~ 20 MHz for free running lasers). Recently a full - wavelength coverage of 72 nm near 1540 nm has been realized for a monolithic diode laser using a sampled-grating DBR (SG-DBR) structure [Cold00].

Table II lists commercially available diode lasers suitable for use as DFG pump sources.

Table II. Overview of diode lasers suitable for cw-DFG applications. DBR, Distributed–Bragg-Reflector; SG-DBR, Sample-Grating-DBR; SSG-DBR, SuperStructure Grating-DBR; DFB, Distributed-Feed-Back; SSG-DFB, SuperStructure Grating-DFB; ECDL, External-Cavity-Diode-Laser.

Diode-based laser	Power (mW)	Wavelength (nm)	Typical linewidth (MHz, 1 sec.)	Tuning	Ref.
Fabry-Perot	1-200	635-865	50-200	< 1 cm^{-1}	[Witt91]
DBR	20	635-680	-	3 nm	[Peze99]
	280	830-1100	-	-	[Majo94]
SG-DBR	2-20	1540	-	40-80 nm	[Cold00]
SSG-DBR	4	1550	-	105 nm	[Ishi93]
	2.7	1560	0.4	40 nm	[Ishi95]
	11	1550	-	62.4 nm	[Ishi96]
DFB	100-400	634-660	-	-	[Peze99]
	430	920	-	-	[Wong97]
	1000	980	-	-	[Wong97]
	130	1310	-	-	[Chen95]
	108	1550	< 2	-	[Chen98]
SSG-DFB	25	1550	< 5	86 nm	[Tohm93]
ECDL	5-20	632-985	< 2	5-20 nm	[New, Sdl]
	5-20	1270-1630	< 2	50-70 nm	[New, Sdl]

2.4.3 Diode pumped solid-state lasers and semiconductor optical amplifiers

Diode-pumped solid state non-planar ring laser (e.g.Nd: YAG) and master oscillator power amplifier (MOPA) can provide cw single-frequency optical power as high as ~1W.

However, the laser wavelength is not tunable, and hence must be used with a tunable laser to achieve wavelength tunability in DFG source [Topf97].

High-power tapered GaA1As semiconductor amplifiers operating near 860 nm (cw single mode power > 1W) [Mehu 93] have been successfully used as DFG pump sources [Simo93b].

By use of injection-locking a high-power A1GaAs laser diode array with a narrow-linewidth external cavity laser as master oscillator, a single - frequency cw output power of ~1W with a spectral linewidth of < 38 kHz and a wavelength tuning range of 13 nm have been reported [Tsuc94].

2.4.4 Fiber amplifiers and lasers

A large variety of rare earth doped optical fiber amplifiers for wavelengths ranging from 900 to 2100 nm (See Table III) with outputs at multi-Watt power levels [Beck99] offer the optimum approach to boost available pump powers to achieve cw DFG powers of >1 mW [Rich00, Rich01, Mats01]. A number of companies offer very robust Yb and Er/Yb optical fiber amplifiers at 1 and 1.5 μm, respectively.

Table III. Near-infrared high-power rare-earth doped fiber amplifier [Beck99]

Dopant	Emission wavelength (nm)	Pump wavelength (nm)	Slope efficiency (%)
Nd	900 - 950, 1050-1100	810	50
Yb	970 - 1160	915 / 975	90
Er	1520 - 1590	980 / 1480	60
Pr	1280 - 1340	980 - 1030	14
Er / Yb	1520 - 1590	975, 1010-1100	45
Tm	1600 - 2100	810 / 1600	36 / 70

2.5. Gaussian pump beams coupling and power conversion efficiency

2.5.1 DFG conversion efficiency

The three-wave nonlinear optical interaction process has been analyzed by Armstrong et al [Arms 62] in 1962. The difference-frequency conversion efficiency has been investigated by Boyd and Kleinman [Boyd68], based on the electric field generated by two focused Gaussian beams. In the case of two collinear Gaussian beams (with powers P_p and P_s at frequencies ω_p and ω_s, respectively) with identical confocal parameters $b = k_p w_p^2 = k_s w_p^2$ (here w is the beam waist), the DFG output power P_i at the diffeence - frequency ω_i can be written as (at zero phase mismatch):

$$P_i = \frac{(16\cdot\pi\cdot\omega_i)^2}{c^3}\cdot\frac{(d_{eff})^2}{n_i\cdot n_s\cdot n_p}\cdot\frac{h(\mu,\xi,\alpha)}{(k_s^{-1}+k_p^{-1})}\cdot L\cdot P_p\cdot P_s\cdot\exp(-\frac{\alpha\cdot L}{2}) \quad (8)$$

Here c is the speed of light in vaccum, n the index of refraction, L the crystal length, d_{eff} the effective nonlinear coefficient, and α is the absorption coefficient of nonlinear medium at the DFG frequency. A focusing function $h(\mu, \xi, \alpha)$ determines the relative DFG conversion efficiency (the optimum focusing position is assumed at the center of the crystal):

$$h(\mu,\xi,\alpha) = \frac{1}{4\cdot\xi}\cdot\int_{-\xi}^{+\xi}d\tau\cdot\int_{-\xi}^{+\xi}d\tau'\cdot\frac{\exp(\frac{b\cdot\alpha}{4}(\tau-\tau'))}{1-\frac{j}{2}\cdot(\frac{1+\mu}{1-\mu}+\frac{1-\mu}{1+\mu})\cdot(\tau-\tau')+\tau\cdot\tau'} \quad (9)$$

with $\mu = k_p / k_s$ and the focusing parameter $\xi = L/b$ which relates the crystal length to the beam size of the pump and signal.

Equation 8 shows typical features for a three-wave optical parametric mixing process:

1.The DFG power is proportional to the nonlinear optical figure of merit, $d_{eff}^2/(n_i n_s n_p)$

2.The output power varies linearly with the product of the input powers. In practice, the efficiency of DFG is dependent on the pump power density incident on the nonlinear optical crystal, while the power density is limited by laser induced damage of the crystal. A large optical damage threshold is thus highly desirable. Recently commercially available ferroelectric material based QPM crystals, such as PPLN, PPRTA, exhibit high laser induced damage thresholds and lead to mW cw DFG powers. In the case of pump sources with low powers, an interacavity DFG technique can be used to enhance pump power levels [Simo95, Petr95].

3. As shown in Figure 10, the h-function reduces to $h\sim\xi$ when using a loose focusing

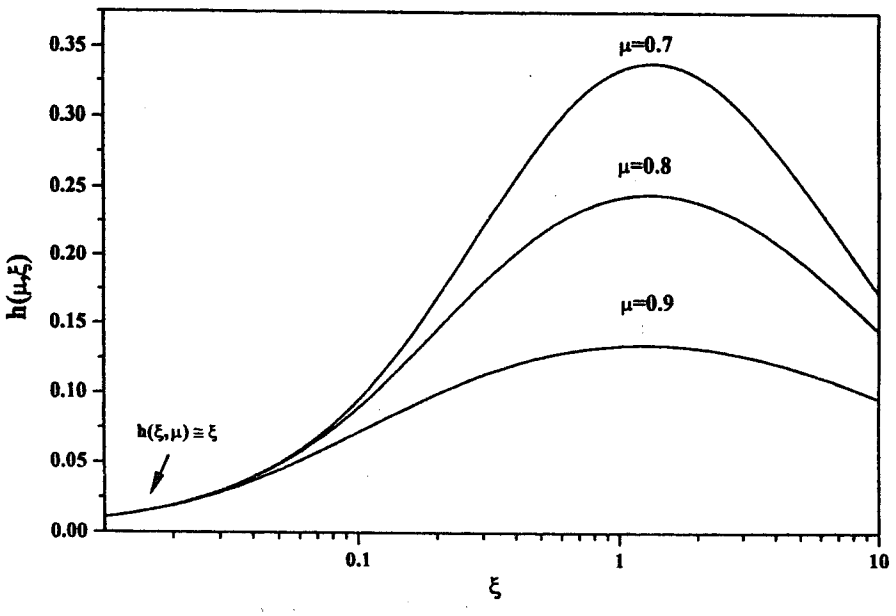

Figure 10. Relative DFG conversion efficiency (h-function) using focused Gaussian beams [Boyd68]

parameter $\xi \sim 0$, which makes the DFG power proportional to L^2, as in the case of the plane-wave approximation; In the case of Gaussian beam coupling, the DFG power varies with L, and reaches a maximum value with an optimum focusing parameter of $\xi \sim 1.3$.

The transverse mode behaviour of the pump laser beams plays also an important role in the coupling of interacting waves, as pointed out in Ref. [Ashk63], TEM_{11} beam mode coupling degrades the nonlinear frequency conversion efficiency by more than a factor of 2 with respect to TEM_{00} mode coupling.

2.5.2. Gaussian pump beams coupling and overlapping

The location of the focused Gaussian beam waist is frequency-dependent and hence the interacting wave efficiency is degraded by a longitudinal chromatic aberration effect. The design of a frequency-independent optical system allows the overlapping of the laser beam waists inside the DFG mixing cystal. A simple telescope system is employed for this purpose [Pitn98]. In order to avoid the complexity resulting from additional optical components and alignment, implementation of a quasi-achromatic Gaussian optical system [Chen99] is convenient, in which the focused beam waist location is quasi-frequency-independent. Significant improvement has been achieved: quasi-frequency-independently overlapping of the beam waists inside the crystal leads to an increase in infrared DFG power by a factor of three.

Optical fiber technology ensured alignment-free pump beam coupling and spatial overlapping, which translates into improved DFG power conversion by a factor of 2 [Rich00].

2.6. Phase-mismatching effects

2.6.1. DFG wavelength tuning

Infrared frequency tuning is usually achieved by scanning one pump laser while the other is held fixed. Figure 11 shows such a frequency scan of the infrared emission from

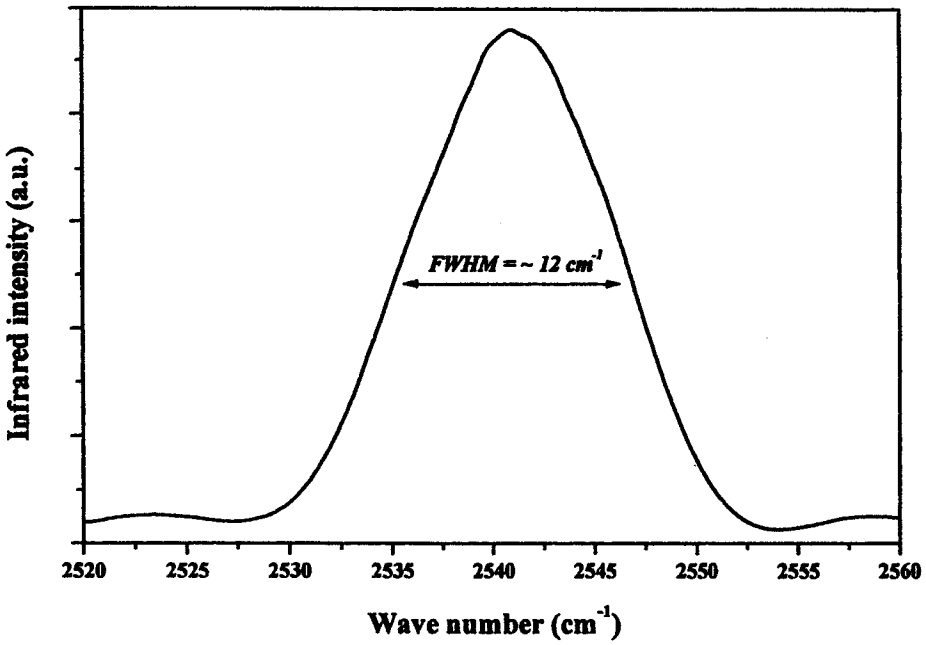

Figure 11. Wavelength-tuning bandwidth of quasi-phase-matched DFG in PPRTA

DFG in PPRTA crystal near 4 μm which is obtained by tuning the pump laser wavelength with the signal laser fixed at ~ 871nm. As is evident from this Figure 11, the infrared wavelength tuning is limited by the phase mismatch condition. A quasi-phase-matched wavelength-tuning bandwidth of ~12 cm^{-1} was observed.

The phase-matching bandwidth BW (FWHM) is inversely proportional to the crystal length and can be written as [Byer77]:

$$BW(cm^{-1}) = \left\{ L_{eff} \left[(n_i - n_s) + \left(\lambda_s \frac{\partial n_s}{\partial \lambda_s} - \lambda_i \frac{\partial n_i}{\partial \lambda_i} \right) \right] \right\}^{-1} \qquad (10)$$

Where L_{eff} is the equivalent crystal length (in cm).

In a DFG evaluation using a 1-mm-thick $AgGaS_2$ plate, phase-matching bandwidth (FWHM) of ~ 22 cm^{-1} was found, which is in agreement with a calculated value of 21cm^{-1} for an effective interaction length of 1.33 mm [Chen98a].

In order to improve the DFG spectral tunability range, usually wavelength combined with temperature tuning is used to maintain the PM condition during large infrared frequency scans [Cana92]. A method of synchronous scanning of the two laser wavelengths was developed to maintain the wavelength-dependent PM condition over a long infrared frequency scan [Chen96]. This was achieved by scanning two laser wavelengths with an appropriate slope ratio : "$\Delta\omega_s/\Delta\omega_i$-to - $\Delta\omega_p/\Delta\omega_i$"

Figure 12 shows an OCS absorption spectrum near 5.3μm obtained from a single laser scan (a) and a synchronous scan (b) over 2 cm^{-1}. In the case of a single scan the infrared frequency tuning bandwidth is limited by phase-mismatching effects to be ~ 0.6 cm^{-1}.

Wide acceptance bandwidth can be obtained when quasi-phase-matching DFG at QPM degeneracy point where $d\Lambda/d\lambda = 0$. In this case the QPM bandwidths are more than two orders of magnitude larger than that observed in BPM-DFG. A bandwidth of 500 nm around 4.3μ m wavelength has been reported for QPM-DFG in PPLN near the degeneracy point [Gold95].

2.6.2. Phase-matched acceptance angle

As in the case of frequency bandwidth, phase-matching sets a limit to the angle acceptance, $\Delta\theta_{BW}$, which can written as [Suth96]:

$$\Delta\theta_{BW}(FWHM) = \frac{5.568\lambda_i n_o^2(\lambda_i) n_e^2(\lambda_i)}{\pi L_{eff} n_e^3(\lambda_i, \theta)[n_o^2(\lambda_i) - n_e^2(\lambda_i)] \sin 2\theta} \qquad (11)$$

The angle acceptance varies inversely with effective crystal length L_{eff}. Figure 13 shows an experimental angle acceptance of DFG in a 5-mm thick GaSe crystal for the angle tuning type I phase-matching condition. The angular acceptance bandwidth (FWHM), limited by phase-mismatch effects, was ~ 0.5° at 9.45 μm wavelength.

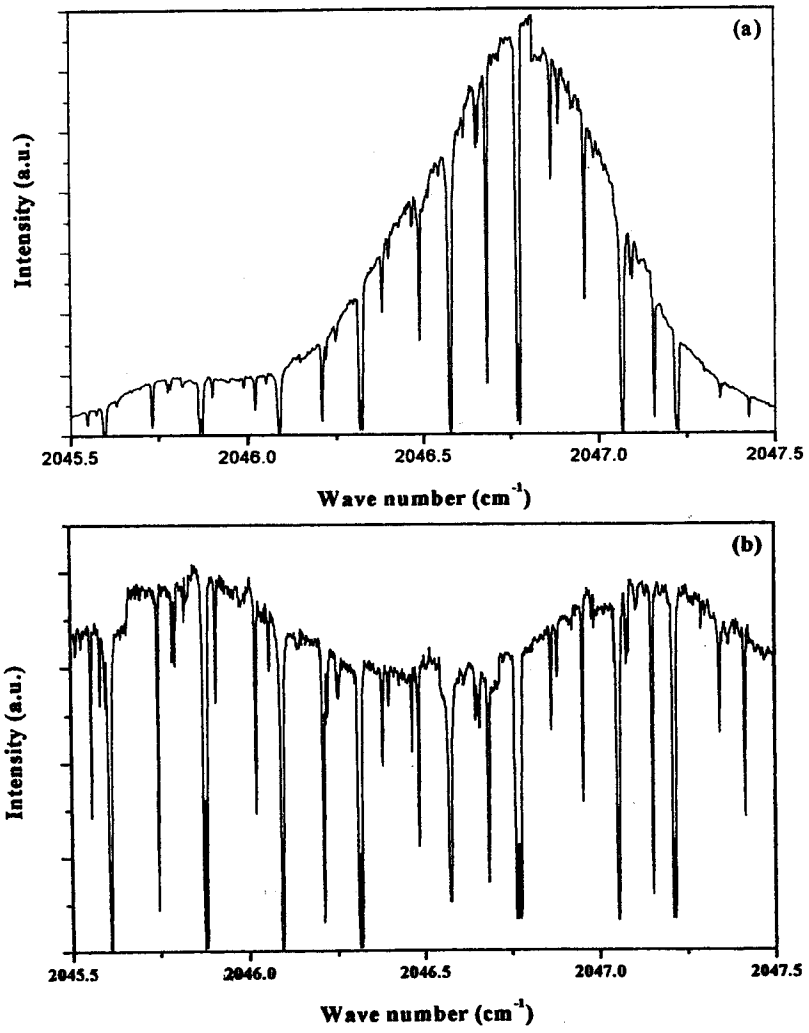

Figure 12. OCS spectrum over 2 cm^{-1}, obtained using: (a) a single laser scan, and (b) a synchronous scan.

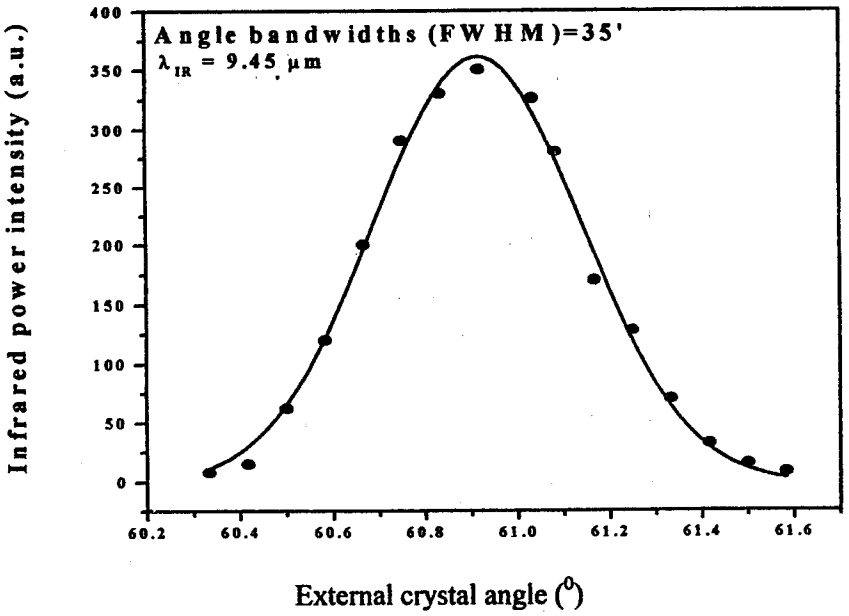

Figure 13. Acceptance angle for DFG in a GaSe crystal for angle tuning the type I phase-matching condition. The angle acceptance bandwidth (FWHM) of ~ 0.5° was observed at 9.45 μm.

3. Difference-frequency generation schemes

3.1. DFG configurations

Different nonlinear optical materials combined with different phase-matching schemes and optical designs were implemented for coherent infrared source generation ranging from 3.5 to 19μm.

A typical schematic diagram of the DFG architecture is shown in Fig. 14. Two Ar^+ laser-pumped cw Ti:Sapphire lasers (Autoscan 899-29, Coherent Inc.) were employed as convenient and versatile laboratory DFG pump sources with an absolute accuracy and reproducibility of frequency measurements of 200 MHz and 50 MHz respectively. Present technology is based on a high power frequency doubled Nd:YAG laser pump source instead of an Ar^+ laser.

The two laser beams were collinearly focused onto a nonlinear optical crystal with a lens of 350 mm focal length (as a compromise between high laser intensities, by use of a lens with short focal length, and a large effective interaction area with a long focus). The laser beam waists were about 50 μm for both lasers. Optical alignment was achieved using a pin-hole technique, and was checked by a beam analyzer camera. All nonlinear optical crystals were operated at room temperature.

The generated infrared emission was collimated with a 90° off-axis parabolic mirror, and directed to a single pass or multipass gas absorption cell fitted with ZnSe windows. The infrared light emerging from the cell was collected by a 90° off –axis parabolic mirror and focused onto a liquid-nitrogen-cooled HgCdTe photoconductive detector with a 1×1

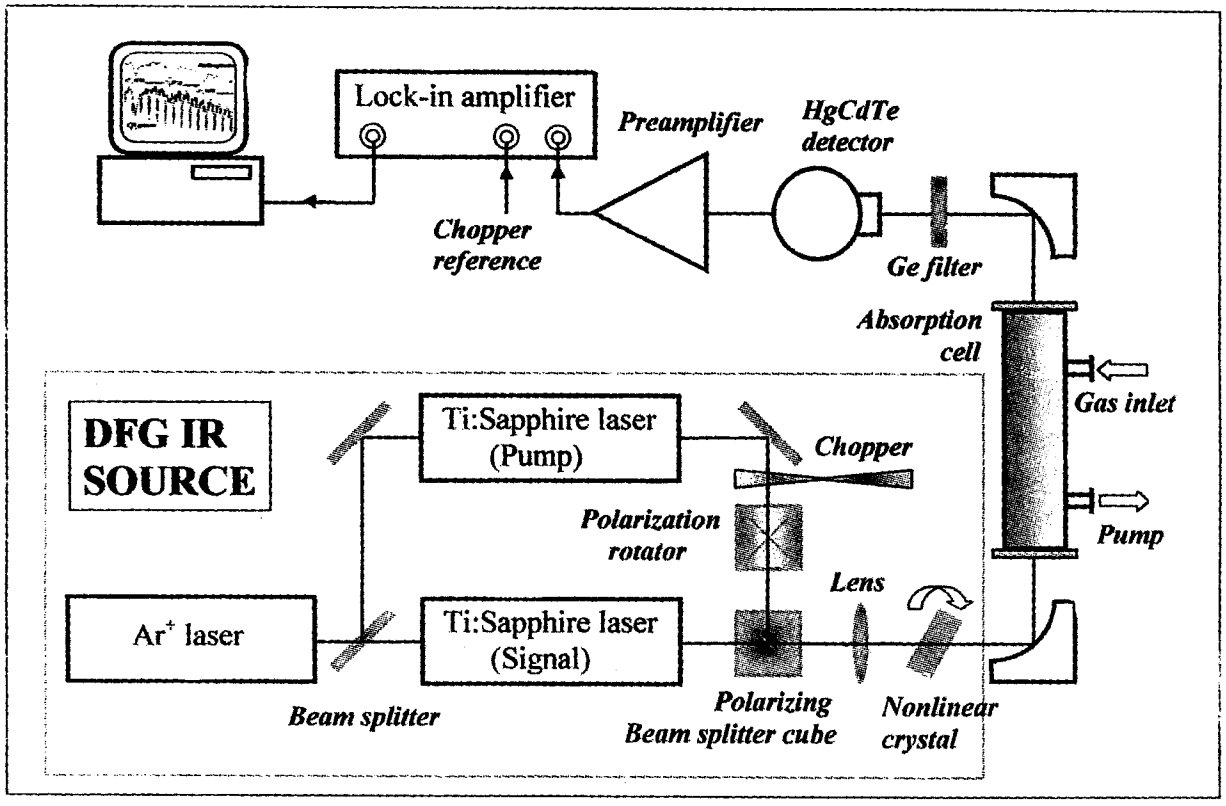

Figure 14. Schematic diagram of typical DFG architecture.

mm^2 active area (EG & G, Judson). A 1-mm thick uncoated germanium (Ge) filter was employed as a long-wavelength pass filter to block unwanted pump and signal laser beams. The filter was set at Brewster's angle to reduce the reflection losses of transmitted infrared beam. The output signal from the detector was amplified by a low-noise preamplifier and fed to a lock-in amplifier.

3.2. Birefringently phase-matched difference-frequency generation (BPM-DFG)

3.2.1 DFG in $AgGaS_2$ by wavelength tuning [Chen96, Chen98a]

Silver thiogallate ($AgGaS_2$) is an effective nonlinear optical crystal frequently used for a DFG infrared source for spectroscopic application in the spectral region from 4 to 18 μm [Cate98]. $AgGaS_2$ is a negative uniaxial crystal ($n_o > n_e$). Its optical transparency is usually reported from 0.47 to 13 μm. In fact, there is a two-photon absorption around 14 μm, and its transparency increases again beyond 15 μm [Chem71, Bhar72, Seym76]. This optical transparency region is suitable for use with commercially available visible-near infrared lasers as pump sources for birefringent PM. A silver thiogallate crystal of 4 mm × 4 mm × 42.5 mm in size (Cleveland Crystal, Inc.) was used by Chen et al [Chen96] for infrared generation from 3.8 to 6.5 μm with type I 90° PM. The cut was $\theta=90^\circ$ and $\phi=45^\circ$ (where θ is the angle between the propagation vector and the crystalline c optic axis, and ϕ the azimuthal angle between the propagation vector and the xz crystalline plane). The corresponding nonlinear effective coefficient can be written as:

$$d_{eoo} = d_{36} \sin\theta \sin 2\phi \tag{12}$$

As type I birefringent PM requires orthogonal polarization (see equation 13), and both lasers were initially vertically polarized, a polarization rotator was used to rotate the polarization of the signal laser by 90° so that this polarization was matched to the b axis of the crystal (as o-ray), and that of the pump laser beam maintained vertical and matched to the c axis (as e-ray). The two orthogonally polarized laser beams were spatially overlapped, made collinear in a polarizing beamsplitter cube, and focused inside the crystal.

$$\frac{n_i^o}{\lambda_i} = \frac{n_p^e}{\lambda_p} - \frac{n_s^o}{\lambda_s} \tag{13}$$

Two laser combination were used: a DCM dye (635-740 nm) and a short-wavelength Ti:Sapphire (700-800 nm) laser pumped DFG for the infrared wavelength from 4.7 to 6.5 μm, and short- and mid-wavelength (800-900 nm) configured Ti:Sapphire lasers used fro DFG in the spectral region from 3.8 to 4.5 μm.

Laser wavelength tuning was used for phase-matching DFG in $AgGaS_2$ in the 3.8 to 6.5 μm. Figure 15 shows the experimental type I 90° wavelength-tuned phase-matching characteristics of an $AgGaS_2$ crystal (circles) at room temperature. After reaching thermal equilibrium in the presence of absorption of the incident pump laser power, a stable phase-matching condition was obtained. The temperature effect on the phase-matching characteristics in the $AgGaS_2$ crystal was found to be -0.7 $cm^{-1}/^\circ C$. The pump power induced temperature change was estimated to be 5°C/W. The optimal generation power

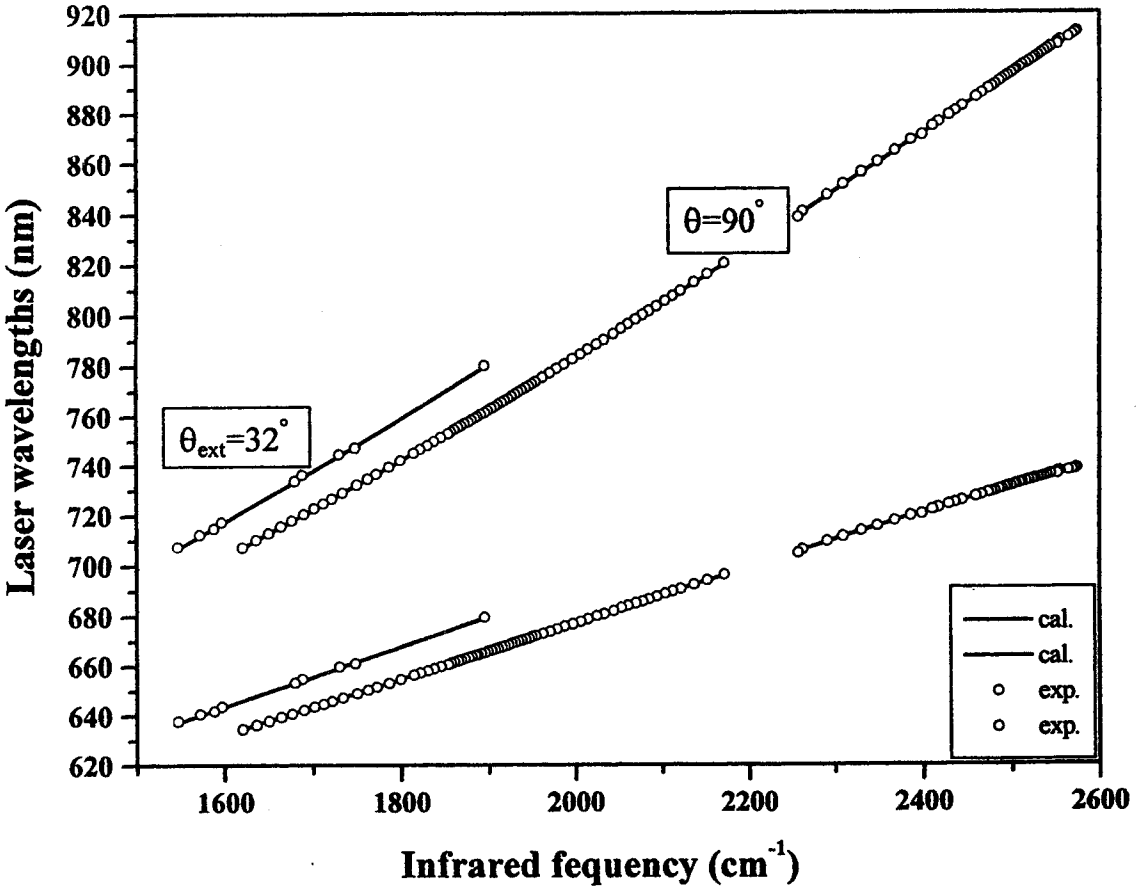

Figure 15. Type I wavelength-tuned phase-matching characteristics of DFG in an $AgGaS_2$ crystal (circles) at room temperature from 3.8 to 6.5 μm, compared with calculated values (solid curves) based on Sellmeier equation given in [Chen99].

conversion efficiency can be approximated as:

$$\eta(\mu W/W^2\cdot cm)=\frac{2.66\times10^6}{\lambda_s(nm)\cdot\lambda_i^2(\mu m)} \tag{14}$$

In a 4.25-cm-long $AgGaS_2$ crystal pumped by 400 mW total power, the DFG power at 4 μm was 17.4 μW. This corresponds to a conversion efficiency of 125 μW/(W^2.cm). Compared with a predicted value of 185 μW/(W^2.cm), the experimental conversion efficiency is ~ 67.5% of the theoretical value.

With a DFG pump configuration consisting of a cw DCM dye and Ti:Sapphire laser, infrared radiation was generated from 4.6 to 6.2 μm in $AgGaS_2$ crystal for type I 90° phase-matching. The phase-matchable infrared spectral coverage can be extended by using a crystal angle tuning technique (i.e. critical PM):

$$\frac{n_o^i(\lambda_i)}{\lambda_i}=\frac{n_e^p(\theta,\lambda_p)}{\lambda_p}-\frac{n_o^s(\lambda_s)}{\lambda_s} \tag{15}$$

where
$$n_e(\theta,\lambda)=\frac{n_e(\lambda)\times n_o(\lambda)}{(n_o^2\times\sin^2\theta+n_e^2\times\cos^2\theta)^{1/2}} \tag{16}$$

By use of the same laser sources mixed in an 1-mm thick $AgGaS_2$ crystal plate, the infrared spectral coverage was extended to 6.5 μm (Fig. 15) with the external crystal angle fixed at 32° [Chen98b]. In the case of angle tuning, the ray direction is different from the wave-normal direction for an extraordinary wave which will not overlap with the ordinary beam in the interaction length. This will result in a " walk-off" effect. The walk-off angle $\rho(\theta)$ is given as [Dmit97]:

$$\rho(\theta) = \pm \tan^{-1}\left[\left(\frac{n_o(\lambda_s)}{n_e(\lambda_p)}\right)^2 \cdot \tan\theta\right] \mp \theta \qquad (17)$$

In the above mentioned $AgGaS_2$ crystal plate, the theoretically estimated "walk-off" free effective interaction length L_{eff} is 30-mm.

For critical PM in an $AgGaS_2$ crystal, type II (e-e->o) interaction offers a d_{eff}^2 twice as large as that for the type I scheme [Petr98]. However the overlapping of pump beams is degraded by walk-off effect as both pump laser beams are extraordinary waves in this case.

3.2.2. DFG in GaSe by wavelength and angle tuning [Chen98c]

GaSe is a negative uniaxial crystal, and is optically transparent from 0.62 to ~ 20 μm. As a layered crystalline material, it can be only cleaved along the 001 plane (z-cut orientation). The nonlinear effective coefficient for type I interaction can be written as:

$$d_{eoo} = d_{22} \cos^2\theta \sin(3\phi) \qquad (18)$$

with a nonlinear coefficient d_{22} of ~54 pm/V. GaSe is very useful material for DFG at long wavelengths up to ~ 20μm.

A z-cut GaSe crystal of 5 mm thick and 10 mm in diameter (EKSMA Co.) was employed for infrared generation from 8.8 to 19 μm. Angle tuning of the z-axis crystal orientation is necessary for birefringent phase matched DFG, as the crystal was cleaved perpendicularly to its optical axis. For a type I PM interaction the laser polarization of the o-beam (signal) shoud be perpendicualar to the x-axis, and the polarization of the e-beam (pump) should be perpendicular to that of the o-beam (as described in equations 15-16), and shown in Figure 16.

Spectral tunability of infrared radiation from 8.8 to 19 μm was achieved with laser wavelengths tuning (750-820 and 800-900 nm, respectively) combined with angle tuning (44 to 66°) of the z-axis crystal orientation for the type I critical PM contition. An empirical expression [Eckh96] has been used to calculate the phase-matched crystal external angle in function of the pump and infrared wavelength. The maximum generated infrared power was ~ 0.2 μW at ~ 9 μm and several nWs near the crystal absorption edge at ~ 20 μm when pumped by a total laser power of ~ 300 mW from both lasers. The maximum power conversion is ~ 10 $\mu W/(W^2.cm)$. The DFG power decreases rapidly with the wavelength, as shown in Figure 17.

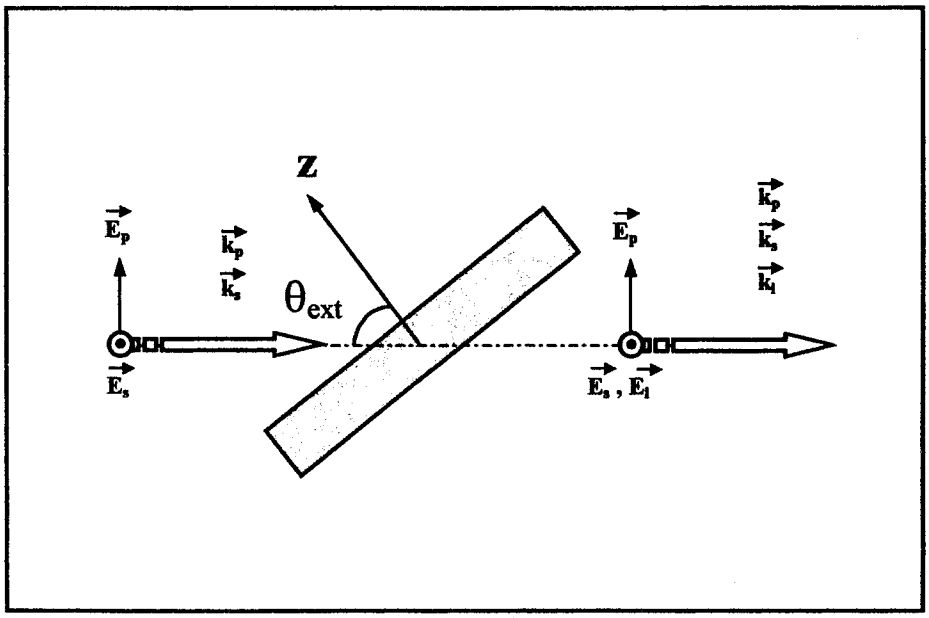

Figure 16. Geometry of GaSe crystal orientation and the field polarizations (top view), where $E_{s,\,p,\,i}$ are the interacting fields, and $k_{s,\,p,\,i}$ the wave vectors.

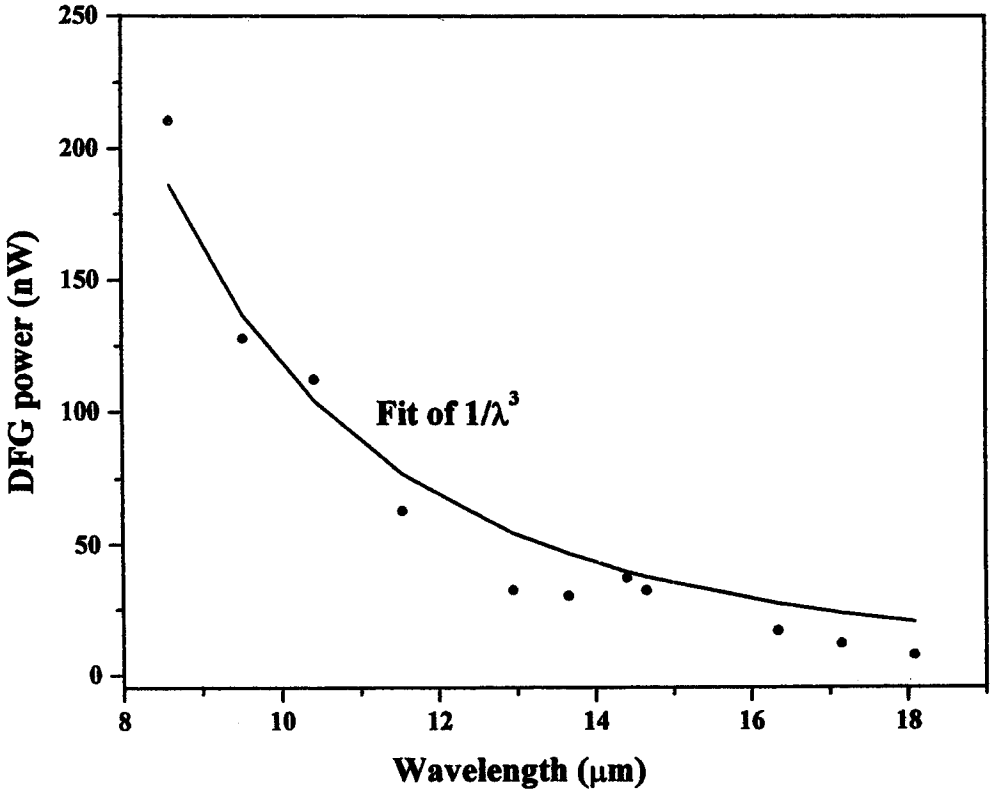

Figure 17. DFG power as a function of the generation wavelength.

3.3. DFG in periodically poled QPM crystals

In a QPM scheme, phase matching does not rely on birefringence, and both pump laser beam polarizations are made parallel to the z-axis of the crystal (e-e->e interaction)

so that the largest nonlinear susceptibility can be used. The periodically modulated nonlinear coefficient can be expressed as a Fourier series [Feje92]:

$$d(z) = d_{eff} \sum_{m=-\infty}^{\infty} G_m \exp(-i \cdot k_m \cdot z) \quad (19)$$

where G_m is the Fourier coefficient of the m-th harmonic,

and $K_m = 2\pi\, m/\Lambda$, the grating vector (20)

For a collinear wave interaction condition, the total wave-vector mismatch can be written as:

$$\Delta k = k_p - k_s - k_i - k_m \quad (21)$$

with m = 1 (corresponding to a grating period with a 50% duty cycle, which optimizes the d_{eff} coefficient), Δk becomes:

$$\Delta k = k_p - k_s - k_i - 2\pi / \Lambda \quad (22)$$

3.3.1. QPM-DFG in periodically poled $LiNbO_3$ (PPLN) [Li98]

Periodically poled lithium niobate (PPLN) crystal is commercially available and widely used for DFG in the infrared region from 3 to 5 μm. PPLN crystals can be engineered for noncritical quasi-phase-matching of any combination of visible or near-IR lasers within the crystal transparency range of 0.2-5.5 μm. Its optical damage threshold is ~ 10 times higher than birefringent crystals, such as $AgGaS_2$ or GaSe.

For example, a cw single frequency tunable Ti:Sapphire laser (800-900 nm) and a diode pumped single frequency Nd:YAG lasr operating at 1064.5 nm can be used as pump sources for DFG. Typically PPLN crystals are available in length up to 50 mm with single and multiple grating periods. For a 20 mm long PPLN crystal with a quasi-phase matching grating period of 22 μm, mid-infrared powers of ~ 2μW at ~5.4 μm were generated with an input power of 500 mW from the Ti:Sapphire laser operating at 885 nm, and 500 mW from the Nd: YAG laser [Li98]. Both pump laser beams were fiber-coupled. The experimental setup is depicted in Fig. 18.

3.3.2. QPM-DFG in periodically poled $RbTiOAsO_4$ (PPRTA) [Chen01a]

Quasi-phase-matched PPRTA offers several distinct advantages compared to other periodically poled ferroelectric optical materials for nonlinear interaction. The optical transparency range for PPRTA extends to about 5.8μ m at long wavelengths (at the zero transmittance level) [Tu99, Dmit97] as compared to 5.5 μm for PPLN, 4.5 μm for PPKTP, and 5.3 μm for PPKTA [Dmit97]. Unlike PPLN that suffers from absorption in the 4-5 μm region, PPRTA has the added benefit of significantly reduced absorption within this region. The nonlinear optical figure of merit, defined as d_{eff}^2/n^3 (where d_{eff} and n are the effective nonlinear optical coefficient and refractive index respectively) of PPRTA is 21.5 $(pm/V)^2$, which is comparable to that of PPLN [27 $(pm/V)^2$. In addition PPRTA possess a high damage threshold of > 400 MW/cm^2 (@ 1064 nm for 10 to 20 ns long pulses), which

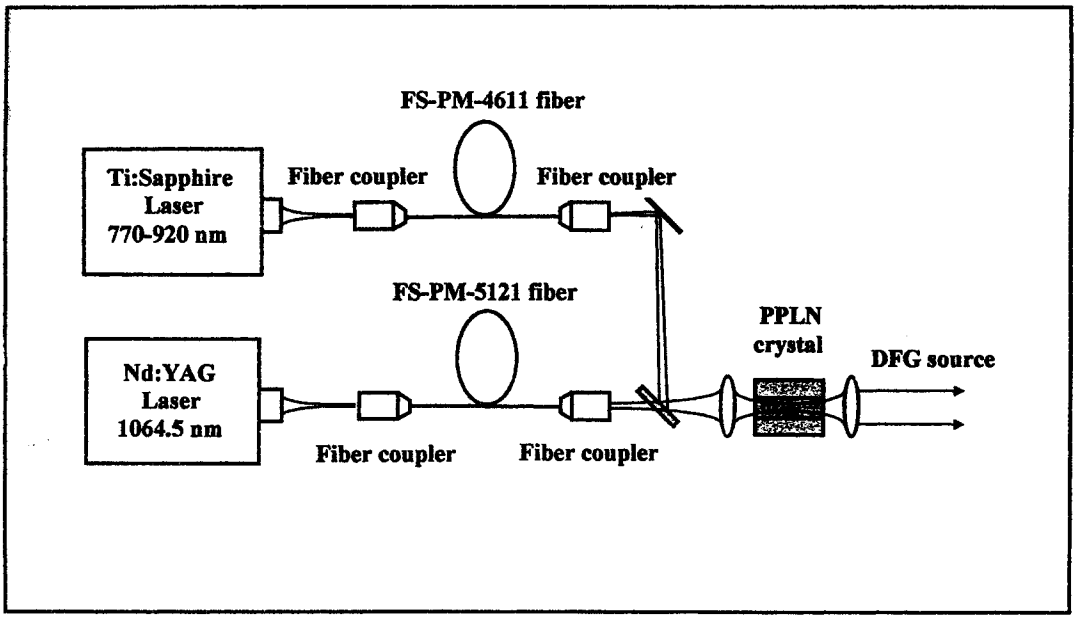

Figure 18. Optical arrangement of a DFG based spectroscopic source

is ~ five times higher than that for PPLN. Furthermore it has ~ 10 times lower coercive field than PPLN for electric poling, which facilitates periodic poling of several mm-thick samples. The last two characteristics are advantageous for nonlinear frequency conversion when using high-power pump sources. PPRTA is thus an attractive alternative to PPLN for nonlinear optical frequency conversion based coherent light generation in the region of 3-5 μm. In addition PPRTA crystal has a significantly higher resistance to photorefractive damage than PPLN, which permits stable operation of the crystal at room temperature.

For example, a PPRTA crystal, 1 mm thick and 20-mm long length with a quasi-phase-matched period of 24.1 μm (Crystal Associates, Inc.) was used in Ref [Chen01a]. Its nonlinear effective coefficient for QPM interaction, $d_m = 2d_{33}/(\pi m)$, can be written as (with m = 1):

$$d_{eff} = 2\, d_{33}/\pi \qquad (23)$$

Infrared radiation is generated with broad wavelength tunability in the 3.4-4.5 μm region with Ti:Al_2O_3 laser wavelengths tunable from 710 to 720 nm, and 847-915 nm, respectively. Infrared radiation powers of 10 μW were produced at 4 μm by mixing Ti:Al_2O_3 lasers operating at 871 nm (100 mW) and 713 nm (200 mW), respectively. After correction for Fresnel losses from the optical components in the setup, these pumping conditions yielded a power conversion efficiency of ~ 0.5 mW/(W^2.cm) at room temperature (Fig. 19).

An effective nonlinear coefficient of d_{eff}=11.2 pm/V was derived from the experimental DFG efficiency at 4 μm. The corresponding nonlinear coefficient d_{33} was determined to be 17.5 pm/V, which is slightly higher than the value of d_{33}=15.8 pm/V given in Ref. [Chen94]. A temperature-dependent wavelength tuning parameter as large as -1.02 cm^{-1}/°C was observed, which is comparable with that for PPLN [Jund97] and about two times higher than that for PPKTP[Gibs98]. The large temperature wavelength-tuning

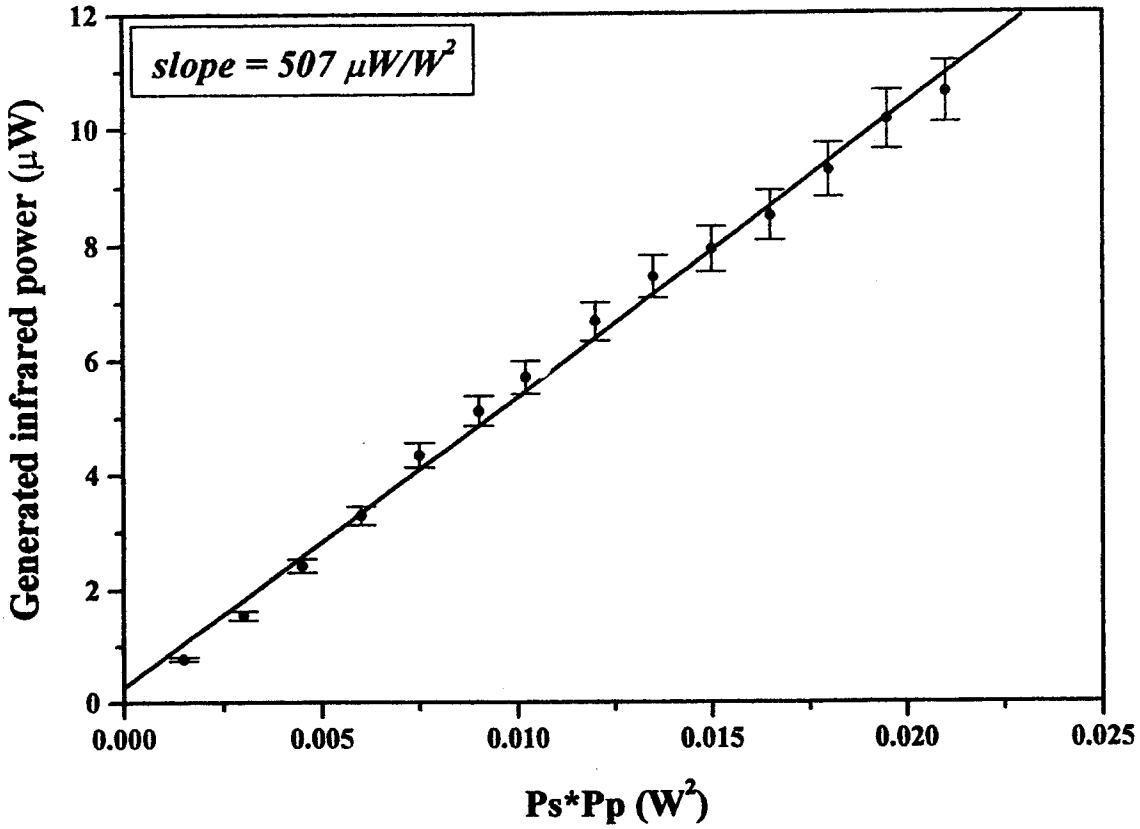

Figure 19. Slope of DFG conversion efficiency in a PPRTA crystal at ~ 4μm: generated infrared power vs. the product of two mixing laser powers.

capability makes PPRTA very attractive for use in widely tunable optical parametric devices.

4. Spectroscopic applications

4.1. High-resolution molecular absorption spectroscopy

4.1.1 High-resolution DFG molecular spectra

Spectroscopic characteristics of the DFG infrared source can be evaluated using high-resolution absorption spectra of carbon dioxide (CO_2) near 4.2 μm, carbonyl sulfide (OCS) near 4.9 μm, nitric oxide (NO) near 5.4 μm, ethylene (C_2H_4) near 10.5 μm, acetylene (C_2H_2) near 13.7 μm, benzene (C_6H_6) near 14.8 μm, and water vapor (H_2O) near 19 μm. Some of these spectra are shown in Figures 20-22, which were obtained at room temperature with a 10-cm long single pass stainless steel absorption cell with ZnSe windows.

A high-resolution DFG spectrum of C_2H_2 of the ν_5 band at < 1 mbar is compared to a FT-IR spectrum obtained with a resolution of 0.2 cm^{-1} in Fig.20.

A spectral comparison of an experimental DFG spectrum of ethylene of the ν_7 band with a simulated spectrum assigned using the HITRAN database [Roth98] is shown in Fig.21.

A direct absorption spectrum of ~ 1 mbar gaseous benzene is shown in Fig.22. The inset is a ~ 0.15 cm^{-1} blowup of the observed ν_4-P (31) line near 662 cm^{-1}. At a benzene

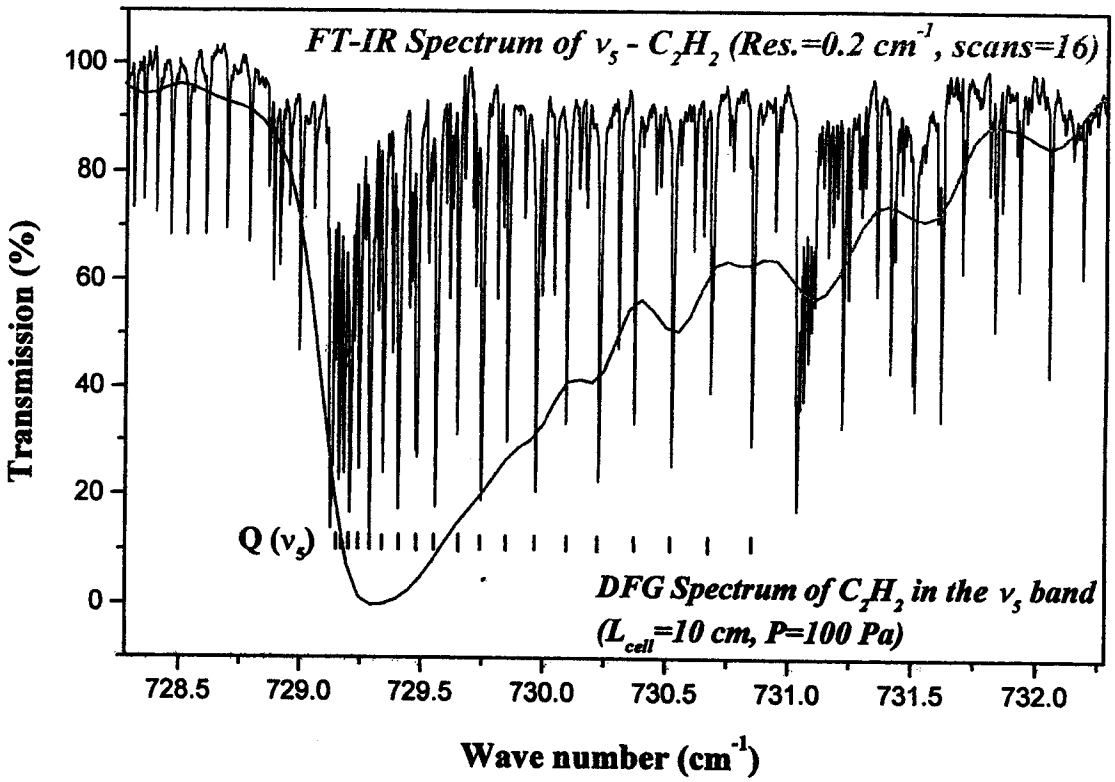

Figure 20. C_2H_2 spectrum of the ν_5 band

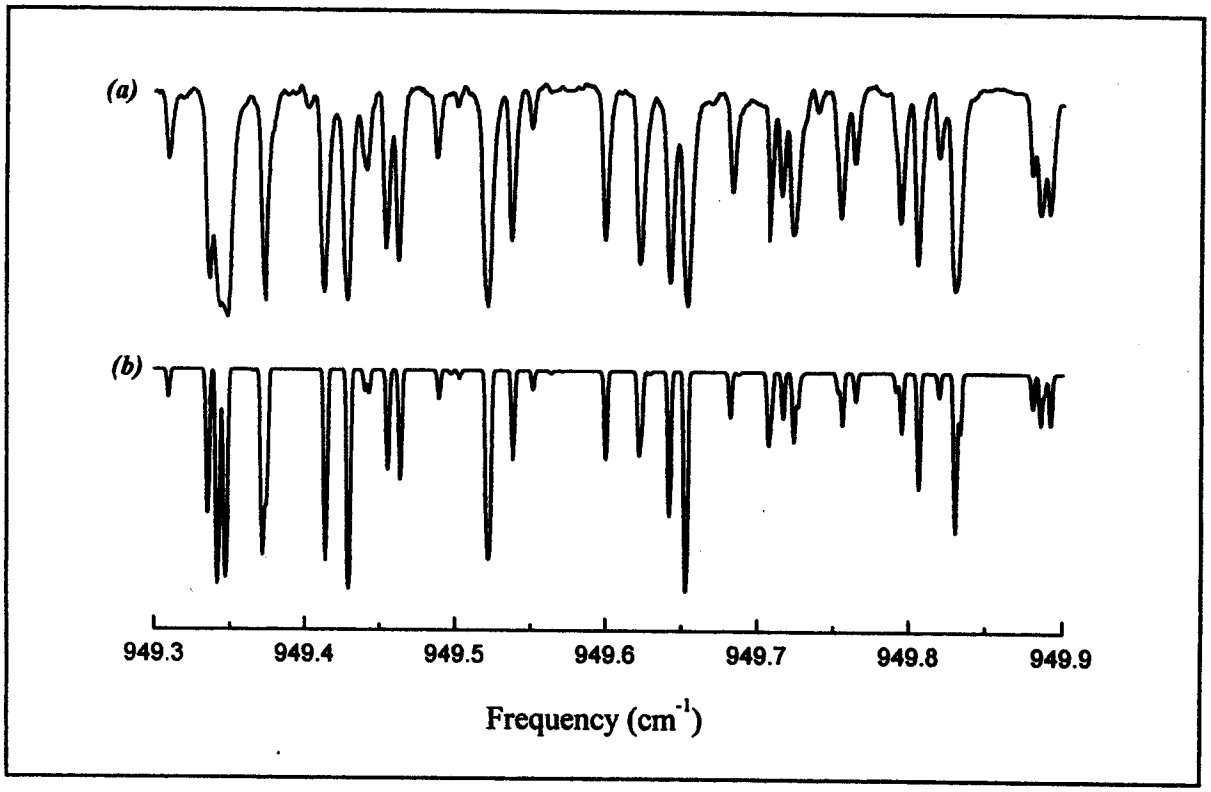

Figure 21. Spectral comparison of : (a) DFG spectrum of ethylene of the ν_7 band at a pressure of ~ 3 mbar and room temperature in a 10-cm long single pass absorption cell, with (b) a simulated spectrum using the HITRAN database [Roth98]

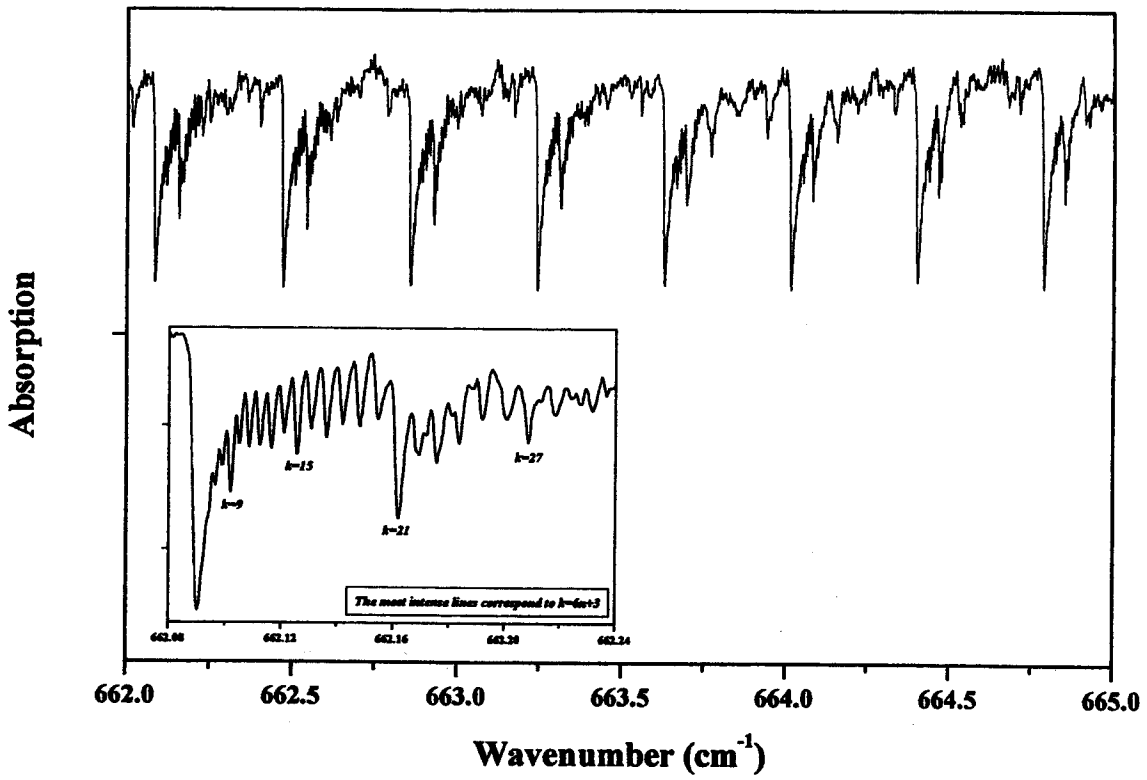

Figure 22. DFG spectrum of the P-branch of the ν_4 band of C_6H_6 (parallel band of A_{2u} vibration ν_4).

vapor pressure of ~ 1 mbar, the K structure of the ν_4 parallel band was resolved for K>7. The intensity variations with the most intense transitions occurring at K = 6n+3 were clearly observed, which is useful for assignment of line transitions. The P (31) transition was assigned using the usual energy expressions for a symmetric top with terms up to the quartic level [Mai89]. The results are shown in Table IV.

Table IV. Observed P (31) transitions of the ν_4 band of benzene.

J'	K'	J"	K"	ν_0 (cm^{-1})	ν_0-ν_c (cm^{-1})
30	7	31	7	662.0964	+0.0001
30	8	31	8	662.0988	+0.0002
30	9	31	9	662.1018	+0.0002
30	10	31	10	662.1048	+0.0001
30	11	31	11	662.1084	+0.0002
30	12	31	12	662.1122	+0.0002
30	13	31	13	662.1164	+0.0002
30	14	31	14	662.1208	+0.0001
30	15	31	15	662.1254	-0.0001
30	16	31	16	662.1308	+0.0001
30	17	31	17	662.1361	-0.0001
30	18	31	18	662.1418	-0.0002
30	19	31	19	662.1481	0.0000
30	20	31	20	662.1545	-0.0001
30	21	31	21	662.1618	+0.0004

4.1.2 Molecular line parameter studies

Laboratory-based measurements of molecular line parameters, such as line broadening and shifting, line strength, line location, and line shape are important in spectroscopic applications ranging from environmental monitoring of trace gases to remote sensing of the atmosphere.

The reliability of spectroscopic measurements using a DFG-based spectrometer can be verified by measuring the air-broadening linewidth of the P (21) line of the ν_5 band of acetylene. Figure 23 depicts pressure-induced broadening and shift of the ν_5- P (21) line of C_2H_2 near 679.71cm^{-1}.

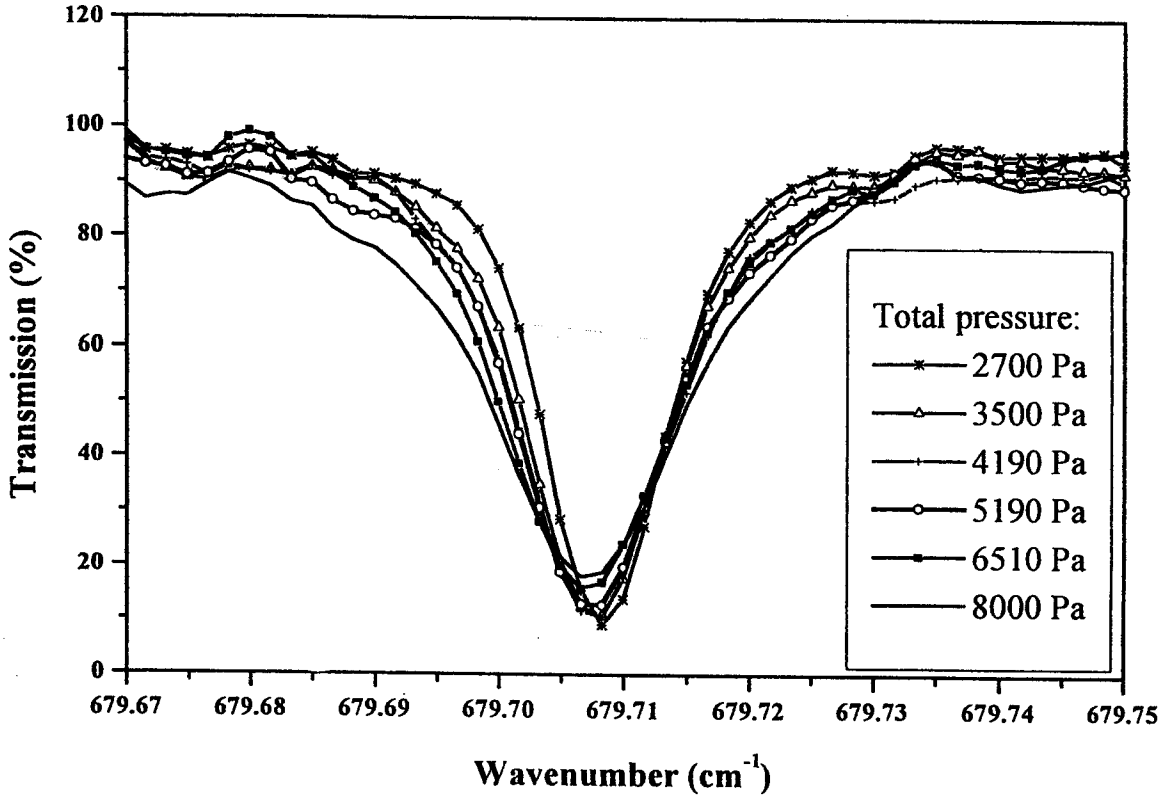

Figure 23. Pressure-induced frequency shift and line broadeningof the P (21) line of C_2H_2 of the ν_5 band near 14.7 μm.

A measurement of the pressure broadening coefficients of the R(15/2) NO lines in a mixture of NO in N_2 was made with a PPLN based DFG spectrometer, since previously reported data are in 30% disagreement with each other [Neis87, Houd83, Phil86, Ball88]. The lines of R (15/2) 1/2 e, f and R (15/2) 3/2e, f were pressure broadened at a temperature of 296 K at N_2 gas pressure of 0, 5,10, 30, 50, and 100 Torr, respectively. The line shape was fitted to a Voigt function with a Gaussian width fixed at a value that was experimentally determined from a pure NO line measurement at a pressure of ~10 mTorr. The measured pressure broadened linewidth coefficients are summarized in Table V and compared with two previously reported data [Neis87, Houd83].

In trace gas detection, a precise knowledge of molecular spectral line parameters is necessary for accurate concentration measurement by means of laser absorption

Table V. Pressure broadening coefficients of the R (15/2) NO lines

Transition: 1 - 0	Parity	1000 x γ (cm^{-1}/atm)		
		Present work	[Neis87]	[Houd83]
$R(15/2)_{1/2}$	e	57.2 (0.8)	49.3 (0.7)	60.8 (6)
$R(15/2)_{1/2}$	f	52.8 (3.2)	49.3 (0.7)	60.8 (6)
$R(15/2)_{3/2}$	e, f	54.9 (3.0)	57.9 (1.5)	62.3 (6)

spectroscopy. However the line parameters of many organic compounds are not available in the GEISA [Jacq99] or HITRAN [Roth98] spectroscopic data bases, and hence original spectroscopic laboratory studies are necessary.

The ν_4 R (6) line C_6H_6 was investigated for air broadening linewidth coefficient measurements. Benzene vapor was buffered by ambient air at room temperature. The pressure-induced linewidths were measured at total pressures varying from 1 to 65 mbars. The pressure-dependent linewidth was determined by fitting a Voigt line-shape function to the experimental absorption line, and the air-broadening coefficient γ_{air} was deduced from the regression slope. Figure 24 shows a plot of the linear dependence of the linewidth of the ν_4 R(6) line on pressures. An air-broadening coefficient γ_{air} (FWHM) of 0.2385± 0.0041 cm^{-1} /atm was determined at 291 K [Chen01b].

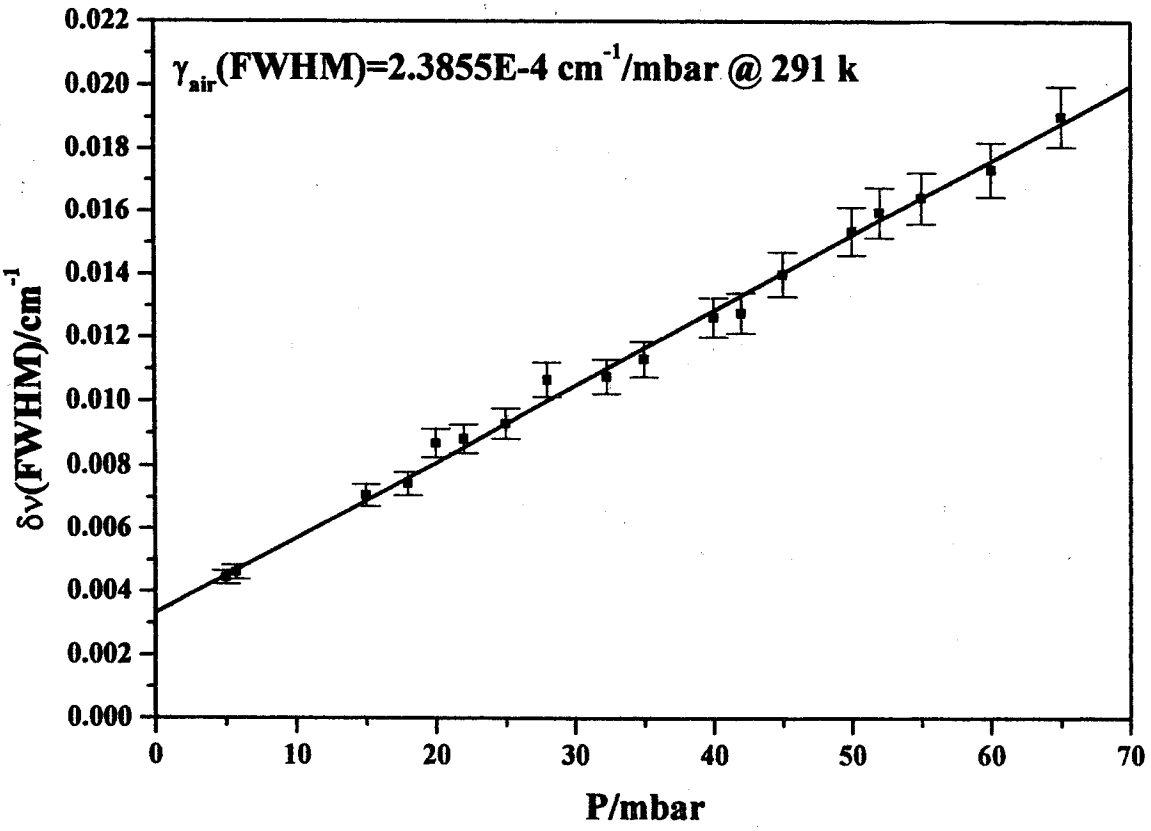

Figure 24. Pressure dependences of the linewidth of the ν_4 R (6) C_6H_6 line.

4.2. Trace gas absorption spectroscopy

The increasing need for in situ characterization and real time quantification of pollutant species has led to the development of spectroscopic monitoring techniques for stack and open-air environmental sensing, industrial process control, remediation activities, and the support of regulatory activities. In the mid-infrared fingerprint region from 3 to 20 μm, most molecular pollutants exhibit fundamental vibrational-rotational absorption bands with molecular specific absorption pattern. A measurement of a specific molecular absorption spectrum allows the identification of gas species and quantification based on the Beer- Lambert law. Such an analysis is usually carried out by least –squares fitting of the observed absorption line(s) using molecular line parameters. Infrared laser absorption spectroscopy offers the advantage of highly selective in situ and real time concentration measurements with detection sensitivities in the ppm (part in 10^6) to sub-ppt (part in 10^{12}) range. Broadly tunable infrared sources permit multi-components detection of atmospheric trace gases and toxic organic chemical species.

4.2.1. Examples of monitoring of atmospheric trace gas species

(1) Water vapor in air [Chen98a]

The H_2O vapor trace was monitored, using a spectroscopic source based on DFG in an 1-mm thick $AgGaS_2$ crystal plate, over an 50-cm open laboratory path between the crystal and the infrared detector. The concentration of H_2O vapor in an air-conditioned laboratory air at room temperature was found to be ~6500 ppm using direct absorption spectroscopy. The relative precision of concentration measurements is ~ 1%.

(2) Carbon dioxide in ambient air [Chen01a]

Measurements of the absorption spectrum of the ν_3 band of carbon dioxide (CO_2) in ambient air were carried out using the QPM-PPRTA based infrared source described in Section 3.3.2. The spectrum shown in Figure 25 (a, top line) was measured, with a ~10 cm^{-1}/scan, at room temperature and atmospheric pressure in an open optical path of 22.5-cm between the crystal and the infrared detector. Fig.25 (a, bottom line) shows a Hitran database [Roth98] simulation of a 350 ppm CO_2 absorption in ambient air. Fig. 25(b) is a high resolution CO_2 spectrum of the ν_3.P (18) absorption line.

(3) Nitric oxide [Li 98]

Nitric oxide (NO) is an biomedically and environmentally important trace gas. It has been demonstrated that NO concentration in human breath can signal asthmatic conditions, HIV infection, brain and heart activities and smoking habits. NO is also one of the major component of industrial smog, as well plays an important role in processes that reduce the concentration of stratospheric ozone. Automobile and diesel engines are the major sources of NO emissions.

The detection of trace amounts of NO was demonstrated using a spectrometer based on DFG in PPLN crystal in an 24-m long absorption cell at 34 Torr with a DFG infrared power of ~2 μW. NO sensitivity of 300 ppb was obtained using the R (15/2) $^2\pi_{3/2}$ - $^2\pi_{3/2}$ (e, f) line near 1903 cm^{-1} with balanced detection.

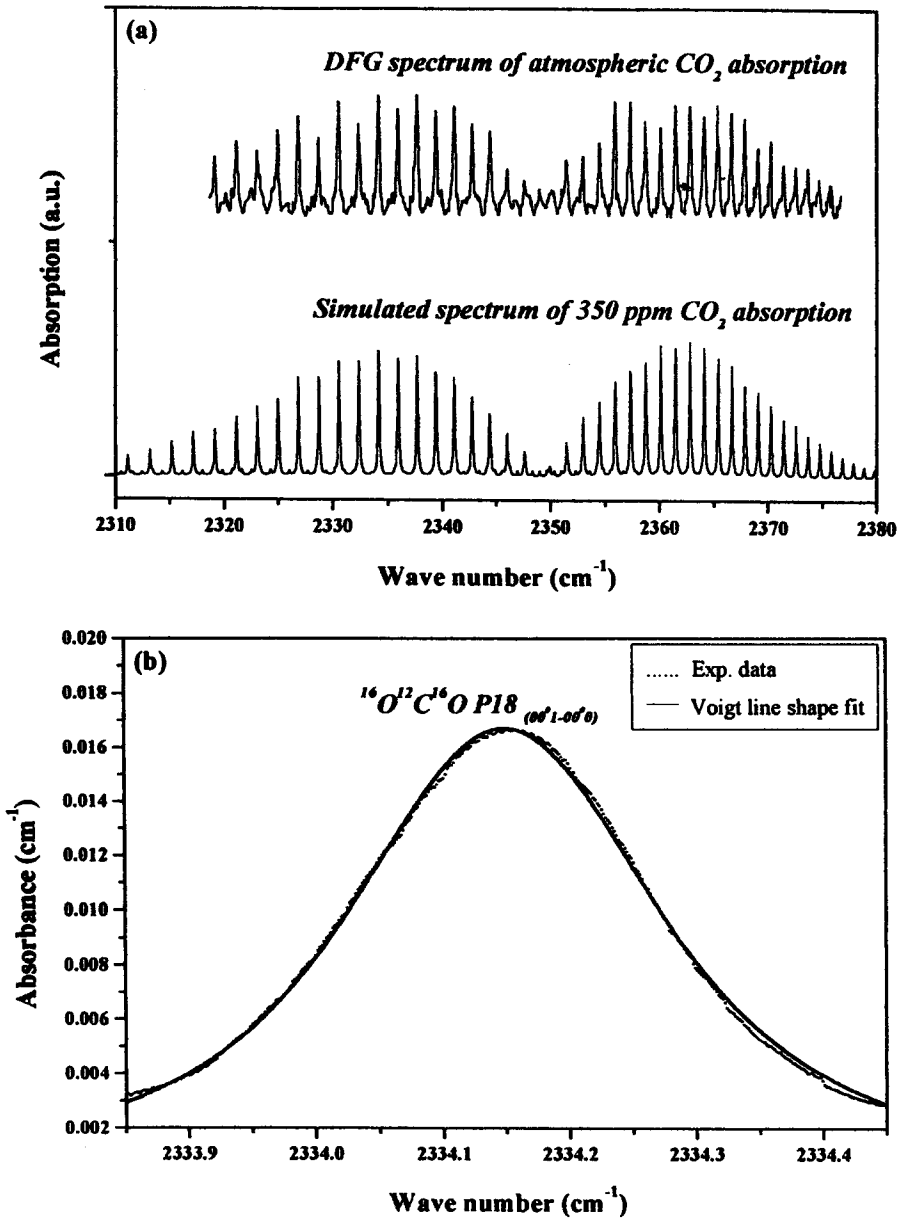

Figure 25. Absorption spectrum of the ν_3 band of carbon dioxide in ambient air.

4.2.2. Spectroscopic analysis of chemical species in the gas phase

There is considerable interest in the identification and quantification of volatile organic compounds (VOCs) levels in the atmosphere and industrial process control. Species include pollutants from combustion, common industrial solvents such as acetone, benzene, carbon tetrachloride, alcohols, and various refrigerant molecules.

(1) Measurement of trace constituent of acetylene [chen00a]

Acetylene (C_2H_2) is a prominent constituent in incomplete combustion products from automobile engines. Under conditions of photochemical oxidation, acetylene is one of the most inert hydrocarbon species, and is considered to be a tracer of polluted urban air masses (5~10 ppb in urban areas). Spectroscopic measurements of C_2H_2 trace

concentration have been performed using the P(21), Q(11), and R(9) lines of the ν_5 band, respectively, in order to investigate optimal detection condition for open path trace-gas monitoring applications: a trade-off choice between higher line absorption strength for sensitive detection and better spectral discrimination from lines overlapping. C_2H_2 concentrations were determined by fitting experimental absorption line(s) to a theoretical line-shape function using line parameters available from the HITRAN database [Roth98]. Sensitive detection of ~1.2 ppm (MDC) was experimentally achieved using the Q (11) line near 13.7μm at a reduced pressure of 168 mbars (to avoid pressure-broadening effects) with a 10-cm long absorption cell. As shown in Fig.26, the R(9) line seems to be a suitable line in terms of absorption strength and absence from spectral interference for spectroscopic detection under atmospheric conditions (at room temperature and atmospheric pressure) with a MDC of ~7 ppm. A comparison of C_2H_2 trace detection using the P(21), Q(11), and R(9) lines of the ν_5 band under different experimental conditions is summarized in Table VI. The concentration measurement is normalized in terms of the concentration-path in ppm-m, and the absorption intensity is expressed in terms of the normalized absorption coefficient in $ppm^{-1}m^{-1}$. The 3σ –detection-limited minimum detectable concentration (MDC) is given with a confidence level of 99.86% assuming a 1 sec. time constant and an optical path of 100-m based on measured noise features dominated by the fluctuations of the spectroscopic probing source.

(2) Benzene concentration measurements [Chen00b]

The feasibility of benzene vapor trace concentration measurements has been demonstrated using mid-infrared difference-frequency laser absorption spectroscopy near

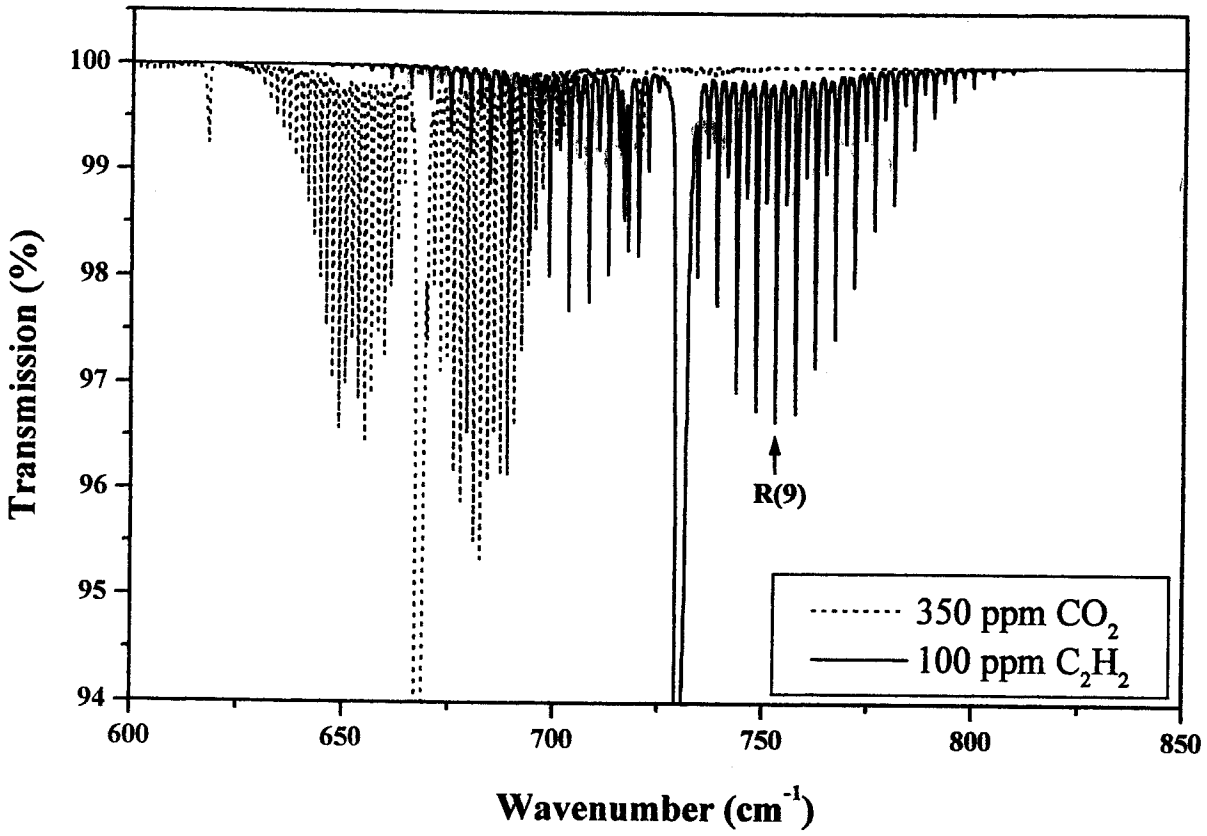

Figure 26. Hitran database-based CO_2-C_2H_2 absorption spectra near 700 cm^{-1}.

Table 6. Comparison of C_2H_2 trace detection using the P(21), Q(11), and R(9) lines of the ν_5 band.

Rotational assignment (ν_5 band)	Transition frequency (cm^{-1})	Line strength (cm/mol.)	Absorption coefficient ($ppm^{-1}\ m^{-1}$)	Measured concentration-path (ppmm)	Pressure (Torr)	MDC* (ppbv)
P (21)	679.7095	1.32^{E}-19	6.65^{E}-4	96.1	760	84.7
Q (11)	729.7380	1.08^{E}-18	2.68^{E}-2	7.7	126	2.4
R (9)	752.6589	6.82^{E}-19	2.88^{E}-3	43.2	760	20.7

14.8 μm. Benzene is an important organic solvent widely used as an additive gasoline that is emitted into the atmosphere by engine exhausts.

The ν_4- fundamental A_{2u} band exhibits the strongest absorption in the infrared resulting from an out-of plane hydrogen motion. However the ν_4 band is strongly interfered with atmospheric CO_2 absorption lines. Hence a high-resolution spectroscopic measurement is necessary for discrimination of benzene absorption from CO_2 interference. As shown in Figure 27(a), sensitive C_6H_6 concentration measurement can be made using strong absorption lines between two adjacent strong CO_2 absorption lines separated by ~1.5 cm^{-1}. In this manner benzene absorption lines of the ν_4 R (6) and $\nu_4 + \nu_{20} - \nu_{20}$ R (9) near 676.62 cm^{-1} were selected.

Fig. 27 (b) depicts a 173 ppm C_6H_6 trace absorption spectrum of the ν_4 R (6) and $\nu_4 + \nu_{20} - \nu_{20}$ R (9) near 676.62 cm^{-1} at room temperature and ~ 40 mbar (a reduced pressure in the range of some tens mbar was used in order to reduce pressure-induced spectral interference effects), acquired by the DFG based absorption spectrometer. The solid line is a Voigt profile fitted to the absorption lines (dots). The residual from the Voigt line-shape is shown below the C_6H_6 spectrum. The signal-to- noise ratio of ~ 15 deduced from this spectroscopic measurement corresponds to a minimum detectable concentration of ~ 11.5 ppm with a 10-cm long single pass cell. Increased sensitivity at the sub-ppm level should be attainable using long path absorption spectroscopy in combination with signal filtering and enhanced data acquisition techniques.

5. Discussion and future outlook

The development of tunable continuous-wave (cw) laser source of coherent radiation in the infrared is of considerable interest for many applications, such as: *environmental applications* to green house gas monitoring, atmospheric gas analysis, detection of explosives or fugitive emissions from illicit drug-manufacturing sites, monitoring of fires and gas leakage, vehicle exhaust emission sensing, combustion-generated pollutant source monitoring, catalytic converter diagnostics; *industrial applications for* chemical process control, monitoring of industrial risks, semiconductor process diagnostics; *medical applications* to glucose detection, breath analysis, diagnostics of ulcers, cardiovascular diseases, colon and lung cancer; *spectroscopic applications* to high-resolution and

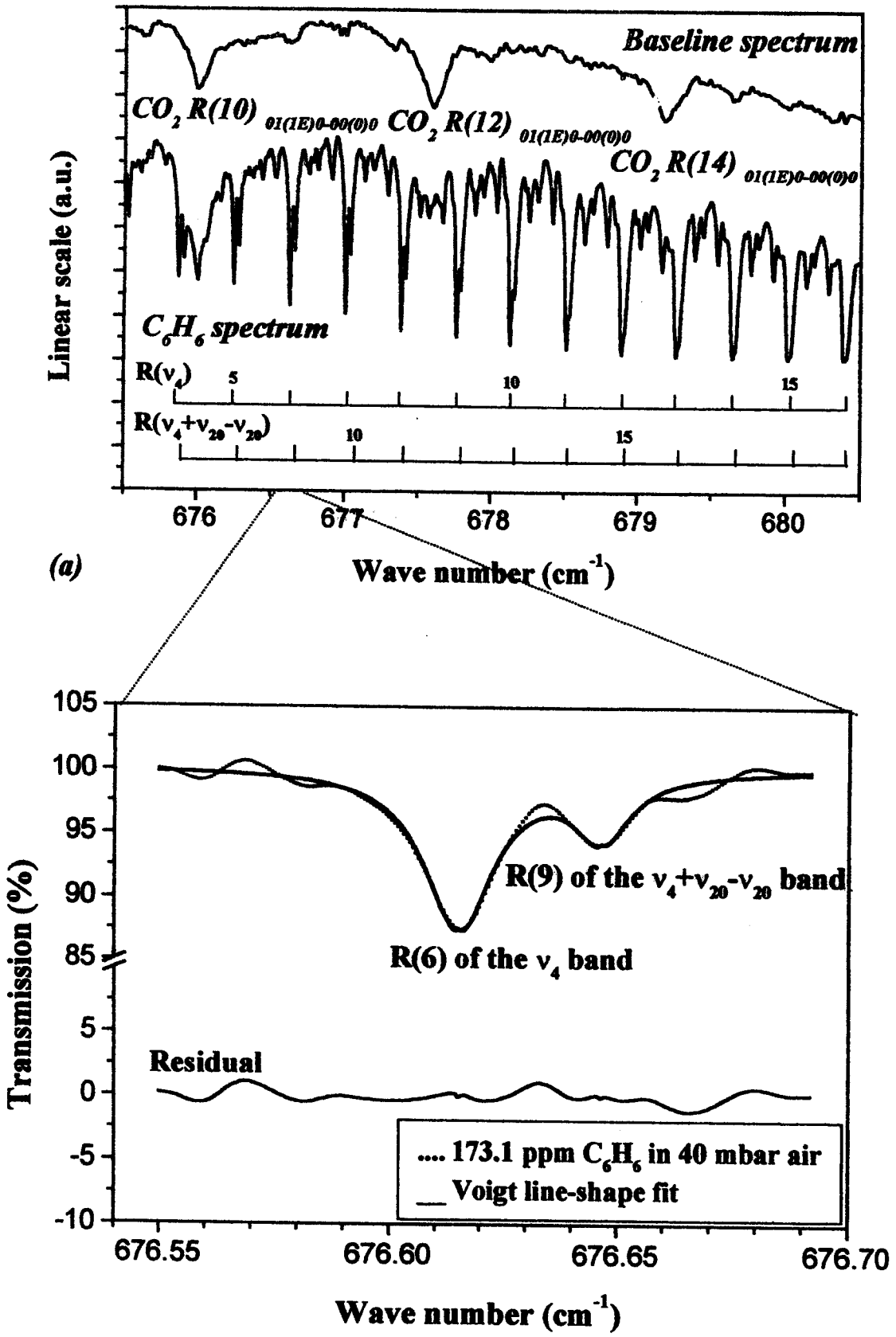

Figure 27. DFG spectra of benzene: (a) Background baseline spectrum indicating the presence of atmospheric CO_2 absorption, and gaseous benzene spectrum at ~1 mbar pressure with interfering CO_2 absorption lines; (b) 173-ppm benzene absorption spectrum of the ν_4 R (6) and $\nu_4 + \nu_{20} - \nu_{20}$ R (9) at 40-mbar, its fit to a Voigt lineshape function, and the associated residual.

precision spectroscopy, reaction kinetic studies by time-resolved spectroscopy, study of the terrestrial atmosphere, investigation of environmentally and climatically relevant processes; *military applications* in sensing of toxic gases and biological toxins, infrared counter-measurements; *optical frequency metrology standard and characterization of infrared components* such as frequency response of detectors, fiber dispersion, and optical components.

The development of cw DFG techniques in future should emphasize the following direction in order to keep the DFG sources simple, and with reliable autonomous performance [Rich 01]. This trend will utilize fiber amplifiers and fiber lasers as pump sources and waveguided structures in QPM materials as more efficient frequency conversion devices than bulk crystals.

(1) Frequency conversion efficiency. DFG-based infrared radiation sources that use birefringent nonlinear materials, in particular at long wavelengths, is subject to an important limitation by its relatively low generation power: of ~μWs with a conversion efficiency in the range of 10^{-5} W^{-1} cm^{-1}. Hence a promising development is to use QPM media to phase match optical frequency conversion process. Higher frequency down-conversion efficiencies have been obtained from DFG in QPM crystals. Using QPM-PPLN as frequency conversion devices combined with high-power fiber amplifier, infrared power scaling to the mW level has been achieved at 3.4 μm with a DFG-based sensor [Lanc00, Rich01]. Another approach is the use of waveguided crystal. A normalized conversion efficiency as high as 105% W^{-1} has been reported by Hofmann et al using periodically poled Ti:$LiNbO_3$ channel waveguides as QPM device for cw DFG near 2.8 μm [Hofm99].

Alternatively, intersubband quantum wells are materials suitable for a high conversion efficiently nonlinear process, since the second order nonlinear susceptibility $\chi^{(2)}$ is several orders of magnitude larger than that for bulk media. DFG in intersubband In GaAs/A1As quantum wells has been demonstrated by Chui et al for the spectral region of 8-12 μm [Chui95]. For DFG, a $\chi^{(2)}$ of 12nm/V at 9.5 μm was observed, which is more than 65 times that of bulk GaAs (180 pm/V).

Photonic crystals could be another potential materials for phase-matched nonlinear optical processes using the photonic band gap [Cent00, Cent01]. Near the photonic band edge, an increase in the density of modes and overlap of strong modes occur, and the nonlinear frequency conversion efficiency could be enhanced by several orders of magnitude [Scal97, Haus98]. An order of magnitude enhancement of second-harmonic generation intensity over bulk material has been experimentally observed near the band edge of a ZnS/SrF multiplayer stack [Bala99]. However, so far all investigations have been performed using a pulsed laser pump. For further details, the reader is referred to the relevant provided references.

(2) Extension of cw DFG to long-wavelength infrared spectral region. Infrared radiation by DFG at long-wavelength of ~ 16 μm has been demonstrated in pulsed mode by Zheng et al [Zhen98] in diffusion-bonded-stacked GaAs crystal. More recently cw operation of DFG in orientation-patterned GaAs near 8 μm has been reported by Levi et al [Levi01].

(3) DFG using a single laser. Tunable DFG in MgO-doped periodically poled $LiNbO_3$ crystal by mixing of dual-wavelength pulses emitting from a single Ti: Sapphire laser has been reported by Saito et al [Sait00]. The wide spectral region from 3.6 to 5.6 μm can be tuned with an intracavity acoustooptic tunable filter.

Using widely tunable monolithic diode laser technology [Cold00] combined with intersubband quantum wells phase-matching scheme [Chui95], monolithic QPM wave guided DFG frequency converter should be an attractive compact mid-infrared source.

Aknowledgements

This paper summarizes our DFG experiences and those by others working in the field of developing various DFG configurations. The Laboratoire de Physicochimie de l'Atmosphère participates in the Centre d'études et de Recherches Lasers et Applications, supported by the Ministère chargé de la Recherche, the Région Nord / pas de Calais and the Fonds Européen de Développment Economique des Régions. We acknowledge helpful discussion with Dr. Roger S. Putnam of Aerodyne Research Inc. (Billerica. MA), Drs. R. Kondrotas and D. Kuzma of EKSMA Co. (Lithuania) for helpful advice on DFG in GaSe; Prof. M. Sigrist of ETH (Switzerland), Dr. B. Sumpf of the Max Born Institut, Berlin, Dr. J.-J. Zondy of LPTF (Paris) , and Dr. U. Willer of Technische Universitat Clausthal (Germany).

References

[Arbo96] Arbore, M.A., Chou, M.-H., and Fejer, M. M. 1996, QELS'96 Technical Digest Series 10, 42

[Ashk63] Ashkin., Biyd, G.D., and Dziedzic, J. M. 1963, Phys. Rev. Lett. 11, 14

[Arms62] Armstrong, j. A., Bloembergen, N., Ducuing, J., and Pershan, P. S. 1962, Phys. Rev. 127, 1918.

[Avet99] Avetisyan, Y. H., Babadjanyan, A. J., Kocharyan, K. N., and Nerkarayan, K. H. 1999, J. contem. Phys. 34, 8

[Bala99] Balakin, A. V., Boucher , D., Bushev, V. A., Koroteev, N. I., Mantsyzov, B. I., Masselin, P., Ozheredov, I. A., and shurinow, A. P. 1999, Opt. Lett. 24, 793

[Ball88] Ballard, J., Johnston, W, B., Kerridge, B. J., and Temedios, J. J. 1998, J Mol. Spectrosc. 127, 70

[Bawe90] Bawendi, M. G., Rehfuss, B. D., and Oka, T. 1990, J. Chem. Phys. 93, 6200

[Beck99] Becker, P. C., Olsson. N. A., Simpson, J. R. 1999, Erbium-doped fiber amplifiers: Fundamentals and Technology, Academic Press

[Bhar72] Bhar, G. C., and Smith, R. C. 1972, Phys. Status Solidi A 13, 157

[Bond65] Bond, W. L. 1965, J. Appl. Phys. 36, 1674

[Bord93] Bordui, P. F., and Fejer, M M. 1993, Annu. Rev. Mater. Sci., 23, 321

[Bort94] Bortz, M. 1994, Ph. D. dissertation, Edward L. Ginzton Laboratory, Stanford.

[Bouc99] Boucart, J., Starck, C., Gaborit, F., Plais, A., Bouche, N., Derouin, E., Goldstein, L., Fortin, C., Carpentier, D., Salet, P., Brillouet, F., and Jacquet, j. 1999, IEEE Photon. Technol. Lett. 11, 629

[Boyd68] Boyd, G. D., and Kleinman, D. A. 1968, J. Appl. Phys. 39, 3597

[Boyd92] Boyd, R. W. 1992, Nonlinear optics, Academic Press

[Brav98] Bravetti, P., Fiore, A., Derger, V., Rosencher, E., Nagale, J., and Gauthier Lafaye, O. 1998, Opt. Lett. 23, 331

[Burn94] Burns, W. K.., McElhanon, W., and Goldberg, L. 1994, IEEE Photon. Technol. Lett. 6, 252

[Butc90] Butcher, P. N., and Cotter, D. 1990, the elements of nonlinear optics, Cambridge University

Press
[Byer77] Byer R. L., and Hebst, R. L. 1977, Nonlinear infrared generation, Y.- R. Shen (Ed.), Springer-Verlag
[Cana92] P. Canarelli, P., Benko, Z., Cirl, R. F., and Tittel, f. K. 1992, J. Opt. Soc. Am. B9, 197
[Capa99] Capasso, F., Gmachl, C., Tredicucci, A., Hutchinson, A. L., Sivco, D. L., and Cho, A. y. 1999. OPN 10, 32
[Cate98] Catella, G.C., and Burlage, D. 1998, MRS-Bulletin 23, 28
[Cent00] Centini, M., Sibilia, C., Scalora, M., Rugolo, V., Bertolotti, M., Bloemer, M. J., and Bowden, C. M. 2000, J. Opt. A: Pure Appl. Opt. 2, 327
[Cent01] Centini, M., Scalora, M., D'Aguanno, G., Sibilia, C., Bertolotti, M., Blowemer, M. J., Bowden, C. M., and Haus, J. W. 2001, Opt. Commun. 189, 135
[Chem71] Chemla, D. S., Kupecek, P. J., Robertson, D. S., and Smith, R. C. 1971, Opt. Commun. 3, 29
[Chen94] Cheng, L. K., Cheng, L. T., Galperin, J., Morris Hotsenpiller, P. A., and Bierlein, J. D. 1994, J. Crystal Growth 137, 107
[Chen95] Chen, P. C., J., Ungar, N., and Bar-chaim, N. 1995, Electron. Lett. 31, 1344
[Chen96] Chen, W., Burie, J., and Boucher, D. 1996, Rev. Sci. Instrum. 67, 3411
[Chen97] Chen, W., Burie, J., and Boucher, D. 1997, Looking to the 21st Century, L-F Li et al (Eds.), World Scientific, 362
[Chen98] Chen, T. R., Hsin, W., and Bar-Chaim, N. 1998, Appl. Phys. Lett. 72, 1269
[Chen98a] Chen, W., Przygodzhi, C., Delbarre, H., Peze, P., Burie, J., and Boucher, D. 1998, Infrared Phys. & Technol. 39, 415
[Chen98b] Chen, W., Mouret, G., Burie, J., and Boucher, D. 1998, Int. J. Infrared and Millimeter Waves 19, 409
[Chen98c] Chen, W., Mouret, G., and Boucher, D. 1998, Appl. Phys. B67, 375
[Chen99] Chen, W., Burie, J., and Boucher, D. 1999, Spectrochimica Acta A55, 2057
[Chen00a] Chen, W., Burie, J., and Boucher, D. 2000, IR Phys. & Technol. 41, 339
[Chen00b] Chen, W., Cazier, F., Tittel, F., and Boucher, D. 2000, Appl. Opt. 39,6238
[Chen00c] Chen, W., Burie, J., and Boucher, D. 2000, Laser Physics 10, 521
[Chen01a] Chen, W., Mouret, G., Boucher, D. and Tittel, F. 2001, Appl. Phys. B72, 873
[Chen01b] Chen, W., Cazier, F., Boucher, D. Tittel, F., and Dacies, 2001, Laser Physics, 11, 594
[Chou98] Chou, M. H., Hauden, J., Arbore, M. A., and Fejer, M. M. 1998, Opt. Lett. 23, 1004
[Chu85] Chu, T., and Broyer, M. 1985, J. Phys. 4, 523
[Chui95] Chui, H. C., Woods, G.L., Fejer, M. M., Martinet, E. L., and Harris, Jr., J. S. 1995, Appl. Phys. Lett. 66, 265
[Cold00] Coldren, L. 2000, IEEE J. Select. Topics Quantum Electron. 6, 988
[Dmit97] Dmitriev, V. G., Gurzadyan, G. G., and Nikogosyan, D. N. 1997, Handbook of nonlinear optical crystals, Springer Series in Optical Science 64
[Dunn99] Dunn, M. H., and Ebrahimzadeh, m. 1999, Science 286, 1513
[Eckh96] Eckhoff, W. C., Putnam, R. S., Wang, S., Curl, R. F., and Tittel, F. K. 1996, Appl. Phys. B63, 437
[Eksm] http://www.eksma.It
[Eyre99] Eyres, L. A., Tourreau, P. J., Pinguet, T. J., Ebert, C. B., Harris, J. S., Fejer, M. M. Gerad, B., and Lallier, E. 1999, Quasi-phase matched frequency conversion in all-epitaxial, orientation patterned 200- m-thick GaSe films, Stranford University Annual Report 1998-1999, 37
[Feje92] Fejer, M. M., Magel, G. A. Jundt, D. H., and Byer, R. L. 1992, IEEEE J. Quantum Electron. 28, 2631
[Feni96] Fenimore, D. L., Schepler, K. L., Zelmon, D., Kuck, S., Ramabadran, U. B., Von Ritchter, P., and Small, D. 1996, J. Opt. Soc. Am. B13, 1935
[Fior97] Fiore, A., Berger, V., Rosencher, E., Bravetti, P., and Nagle, J. 1997, OPN 8, 27
[Frad99] Fradkin, K., Arie, A., Skliar, A., and Rosenman, G. 1999, Appl. Phys. Lett. 74, 914
[Frad00a] Fradkin, K., Arie, A., Urenski, P., and Rosenman, G. 2000, Appl. Phys. B71, 251
[Frad00b] Fradkin, K., Arie, A., Urenski, P., and Rosenman, G. 2000, Opt. Lett. 25, 743
[Gibs98] Gibson, G. M., Turnbull, G. A., Ebrahimzadeh, M., Dunn, M. H., Karlsson, H., Arvidsson, G., and Laurell, F. 1998, Appl. Phys. B67, 675

[Gmac00] Gmachl, C., Capasso, F., Kohler, R., Tredicucci, A., Hutchinson, A. L., Sivco, D. L., Baillargeon, J. N., and Cho, A. Y. 2000, circuits & Devices, May, 10

[Gold93] Goldberg, L., Mehuys, D., Surette, M. R., and Hall, D. C. 1993, IEEE J. Quantum Electron. 29, 2028

[Gold95] Goldberg, L., Burns, W., K., and McElhanon, R. W. 1995, Appl. Phys. Lett. 6, 2910

[Grab98] Grabherr, M., Jager, R., Miller, M., Thalmaier, C., Heerlein, J., Michalzik, R., and Ebeling, K. 1998, IEEE Photon. Technol. Lett. 10, 1061

[Hasn00] Chang-Hasnain, C. 2000, IEEE J. Select. Topics Quantum Electron. 6, 978

[Haus98] Haus, J. W., Viswanathan, R., Scalora, M., Kalocsai, A. G., Cole, J. D., and Theimer, J. 1998, Phys. Rev. A57, 2120

[Hiel92] Hielscher, A. H., Miller, C. E., Bayard, D. C., Smolka. J. P., Curl, R. F., and Tittel, F. K. 1992, J. Opt. Soc. Am. B9, 1962

[Hofm99] Hofmann, D., Schreiber, G., Haase, C., Herrmann, H., Grundkotter, W., Ricken, R., and Sohler, W. 1999, Opt. Lett. 24, 896

[Houd83] Houdeau, J. p., Boulet, C., Bonamy, J., Khaayr, A., and Guelachrili, G. 1983, J. Chem. Phys. 79, 1634

[Ishi93] Ishii, H., Tohmori, Y., Yoshikuni, Y., Tamamura, T., and Kondo, Y. 1993, IEEE Photon. Technol. Lett. 5, 613

[Ishi95] Ishii, H., Kano, F., Tohmori, Y., Kondo, Y., Tamamura, T., and Yoshikuni, Y., 1995, IEEE Select. Top. Quantum Electron. 1, 401

[Ishi96] Ishii, H., Tanobe, H., Kano, F., Tohmori, Y., Kondo, Y., Yoshikuni, Y., 1996, Electron. Lett. 32, 454

[Jacq99] Jacquinet-Husson, N., Arie, E., Ballard, J., Barbe, A., Bjo-raker, G., Bonnet, B., Brown, L. R., Camy-Peyret, C., Cham-pion, J. P., Chedin, A., Chursin, A., Clerbaux, C., Duxbury, g., flaud, J.-M., fourrie, N., Fayt, A., Graner, G., Gamache, R., gold-man, A., Golovko, V., Guelachvili, G., Hatmann, J. m., Hilico, J. C., Hillman, J., Lefevre, G., Lellouch, E., Mikhailenko, S. N., Naumenko, O. V., Nemtchinov, V., Newnham, D. A., Nikitin, A., Orphal, J., Perrin, A., Reuter, D. C., Rinsland, C. P., Rosenmann, L., Rothman, L. S., Scott, n. A., Selby, J., Sinitsa, L. N., Sirota, J. M., Smith, A. M. smith, K. m. Tyuterev, V. G., Tipping, R. H., Urban, S., Varanasi, P., and Weber, M. 1999, J. Quant. Spectrosc. Radiat. Transfer 62, 605

[Jund97] Jundt, D. H. 1997, Opt. Lett. 22, 1553

[Klei00] Klein, M. E., Laue, C. K., Lee, D.-H., Boller, K.-J., and Wallenstein, R. 2000, Opt. Lett. 25, 490

[Kron96] Kronfeldt, H.-D., Basar, G., and Sumpf, B. 1996, J. Opt. Soc. Am. B13, 1859

[Lang98] Lang, R. J., Mehyus, D. G., and Welch, D. F. 1998, U. S. Patent 5, 771, 252

[Lanc00] Lancaster, D., Fried, A., Wert, B., Henry, B., and Tittel, F. 2000, Appl. Opt. 39, 4436

[Lee98] Lee, D., Kaing, T., Zondy, J. –J. 1998, Appl. Phys. B67, 363

[Levi01] Levi, O., Pinguet, T. J., Skauli, T., Eyres, L. A., Scaccabarozzi, l., Fejer, M. M., Harris Jr., J. S., Kulp, T. J., Bisson, S., Gerad, B., Becouarn, L., and Lallier, E. 2001, CLEO 2001 Postedeadline Papers, CPD21, Baltimore, MD, USA

[Lfw00] 2000 Buyers Guide, The Industry Sourcebook, Laser Focus Word, December 1999

[Li98] Li, D., Kosterev, A. A., Curl, R. F., Tittel, F. K., Chen, W., and Bamford, D. J. 1998, Opt. Soc. America Technical Digest Series 7, 69

[Lim91] Lim, E. J., Hertz, H. M., Bortz, M. L., and Fejer, M. M. 1991, Appl. Phys. Lett. 59, 2207

[Mai89] Dang-Nhu, M., and Pliva, J. 1989, J. Mol. Spectrosc. 138, 423

[Majo94] Major, Jr., A., O'Brien, S., F. Welch, D., Gulgazov, V., Parke, r., Verdiell, J.-M., and Lang, R. 1994, CELO '94 Technical Digest Series 8, 4

[Mats01] Matsuoka, N., Yamaguchi, s., Nanri, K., Fujioka, T., Richter, D., and Tittel, F. 2001, Jap. J. Appl. Phys. 40, 625

[Mehu93] Mehuys, D., Goldberg, L., and Welch, D. f. 1993, IEEE Photon. Tech. Lett., 5, 1179

[Miss98] Missey, M. J., Dominic, V., Myers, L. E., and Eckardt, R. C. 1998, Opt. Lett. 23, 664

[Mitt91] Mittgrefe, F., Hoogerland, M. D., and Woerdman, J. P. 1991, Meas. Sci. Technol. 2, 304

[Momo96] Momose, T., Wakabayashi, T., and Shida, T. 1996, J. Opt. Soc. Am. B13, 1706

[Myer99] Myers, L. E. 1999, Advances in Lasers and Applications, Finlayson, D. M., B. D. Sinclair

(Eds.), SUSSP Publications, 141
[Neis87] Neiss, T. G., Lovejoy, R. W., and Chackerian, C. 1987, J. Mol. Spectrosc. 124, 229
[Nels74] Nelson, D. F., and Mikulyak, R. M. 1974, J. Appl. Phys. 45, 3688
[New] www.newfocus.com
[Obri99] O'Brien, N., Missey, M., Powers, P., Dominic, V., and Schepler, K. L. 1999, Opt. Lett. 24 1750
[Petr95] Petrov, K., Waltman, S., Curl, R., Tittel, F., and Holberg, L. 1995, Appl. Phys. B61, 553
[Petr96a] Petrov, K., Curl, R., Tittel, F., and Goldberg, L. 1996, Opt. Lett. 21, 1451
[Petr96b] Petrov, K., Goldberg, L., Burns, W. K., Curl, R., and Tittel, F., 1996, Opt. Lett.21, 86
[Petr98a] Petrov, V., Rempel, C., Stolberg, K.-P., Schade, W. 1998, Appl. Opt. 37, 4925
[Petr98b] Petrov, K. P., Ryan, A. T., Patterson, T. L., Huang, L., Field, S. J., and Bamford, D.J. 1998, Appl. Phys. B67, 357
[Petr00] Petrov, K. P., Ryan, A. T., Patterson, T. L., Thomas, T. P. S., Huang, L., Ryan, A. T., and Bamford, A. T. 2000, Appl. Phys. B70, 777
[Peze99] Pezeshki, B., Hagberg, M., Zelinski, M., Zou, S., and Kolev, E. 1999, SPIE 3628, 176
[Phil86] Philips, W. J., and Walker, H. C. 1986, J. Chem. Phys. 85, 3211
[Pine74] Pine, A. S. 1974, J. Opt. Soc. Am. 64, 1683
[Putn98] Putnam R. S., and Lancaster, D. G. 1998, Appl. Opt. 38, 1513
[Rama93] Ramaswamy R. V., and Cao, X. 1993, Nonlinear Opt., 4, 115
[Rich00] Richter, D. 2000, Ph. D. dissertation, Rice University
[Rich01] Richter, D., Erdelyi, M., and Tittel, F. 2001, Advanced Solid State Laser Conf., Seattle, WA (January 28-31)
[Roth98] Rothman, L. S., Rinsland, C. P., Goldman, A., Massie, S. T., Edwards, D. P., Flaud, J. M., Perrin, A., Gamache, R. R., Wattson, R. B., Yoshino, K., Chance, K. V. Jucks, K. W., Brown, L. R., Nemtchinow, V., and Varanasi, P 1998, J. Quant. Spectrosc. Radiat. Transfer 60, 665
[Sait00] Saito, n., Wada, S., Taniguchi, H., Nakamura, M., Urata, Y., and Tashiro, H. 2000, Jap. J. Appl. Phys. Part 1 39, 1767
[Scal97] Scalora, M., Bloemer, M. J., Manka, A. S., Dowling, J. P., Bowden, C. M., Viswanathan, R., and Haus, J. W. 1997, Phys. Rev. A56, 3166
[Scha96] Schade, W., Blanke, T., Willer, U., and Rempel, C. 1996, Appl. Phys. B63, 99
[Sd1] www.sdli. com
[Seit98] Seiter, M., Keller, D., and Sigrist, M. W. 1998, Appl. Phys. B67, 351
[Seym76] Seymour, r. J., and Zernike, F. 1976, Appl. Phys. Lett. 29, 705
[Shoj97] Shoji, I., Kondo, T., Kitamoto, Shirane, M., and Ito, R. 1997, J. Opt. Soc. Am. B14, 2268
[Simo93a] Simon, U., Miller, C. E., Bradley, C. C., Hulet, R. G., Curl, T. F., and Tittel, F. K. 1993, Opt. Lett. 18, 1062
[Simo93b] Simon, U, Tittel, F. K., and Goldberg, L. 1993, Opt. Lett. 18, 1931
[Simo95] Simon, U, Waltman, S., Loa, I., Tittel, F. K., and Goldberg, L. 1995, J. Opt. Soc. Am. 12, 323
[Sump98] Sumpf, B., Rehle, D., Kelx, T., and Kronfeldt, H.-D. 1998, Appl. Phys. B67, 369
[Suth96] Sutherland, R. L. 1996, Handbook of nonlinear optics, Marcel Dekker, Inc
[Tohm93] Tohmori, Y., Kano, F., Ishii, H., Yoshikuni, Y., and Kondo, Y. 1993, Electron. Lett. 29, 1350
[Topf97] Topfer, Th., Petrov, K. P., Mine, Y., Jundt, D., Curl, R. F., and Tittel, F. K. 1997. Appl. Opt. 36, 8042
[Tsuc94] Tsuchida, H. 1994, Opt. Lett. 19, 1741
[Tu99] Tu, C., Katiyar, R., Schmidt, V., Guo, R., and Bhalla, A. 1999, Phys. Rev. B59, 251
[Turn00] Turnbull, G. A., McGloin, D., Lindsay, I. D., Ebrahimzadeh, M., Dunn, M. H. 2000, Opt. Lett.25, 341
[Voge01] Vogel, P., and Ebert, v. 2001, Appl. Phys. B72, 127
[Wer198] Werle, P. 1998, Spectrochimica Acta A54, 197
[Wong97] Wong, V. V., DeMars, S. D., Schoenfelder, A., and Lang, r. J. 1997, LEOS '97 Conf. Proc. 2, 484
[Wilm99] Wilmsen, C., Temkin, H., and Coldern L. A. 1999, Vertical-cavity surface-emitting lasers. Cambridge University Press
[Yoo96] Yoo, S. J. B., Caneau, C., Bhat, R., Koza, A. A., Rajhel, A., and Antoniades, N. 1996, Appl.

Phys. Lett. 68, 2609
[Zern73] Zernike, F., and Midwinter, J. E. 1973, Applied nonlinear optics, John Wiley & Sons
[Zhen98] Zheng, D., Gordon, L. A., Wu, Y. S., Feigelson, R. S., Fejer, M. M., Byer, R. L., and Vodopoyanov, K. L. 1998, Opt. Lett. 23, 1010
[Zond98] Zondy, J. –J. 1998, Opt. Commun. 149, 181